5-2017

Mobile Search Strategies and Detection Analysis of Nuclear Radiation Sources

Luyang Wang
Clemson University, luyangw@g.clemson.edu

MOBILE SEARCH STRATEGIES AND DETECTION ANALYSIS OF NUCLEAR RADIATION SOURCES

A Dissertation
Presented to
the Graduate School of
Clemson University

In Partial Fulfillment
of the Requirements for the Degree
Doctor of Philosophy
Electrical Engineering

---

by
Luyang Wang
May 2017

Accepted by:
Dr. Carl W. Baum, Committee Chair
Dr. Harlan B. Russell
Dr. Robert J. Schalkoff
Dr. Yue Wang

Abstract

This work focuses on detection analysis and search strategies for nuclear radiation sources in metropolitan areas with mobile sensor networks. A mobile sensor detecting a stationary nuclear source experiences continually changing statistics. In this work we provide an analysis of the probability of detection of a nuclear source that incorporates these continual changes. We apply the analysis technique to several patterns of motion including linear and circular paths. Analysis is also presented for cases in which there is a significant vertical offset between source and mobile sensor (the three-dimensional problem). The resulting expressions are computationally simple to evaluate and have application to both analysis and simulation of nuclear detection systems in a variety of scenarios. In metropolitan areas, with vehicles equipped with detectors and Global Position System (GPS) devices, we consider the design of a robust detection system to provide consistent surveillance. Various strategies for providing this surveillance with a mobile sensor network are considered and the results are compared. Both time-from-last-visit based algorithms and detection algorithms that utilize both time and probability-of-miss estimates are considered. The algorithms are shown to perform well in a variety of scenarios, and it is further shown that the algorithms that utilize probability information outperform those that do not.

Dedication

I dedicate my dissertation work to my family. A special feeling of gratitude to my loving parents, Linxu Wang and Haixia Lu whose words of encouragement and push for tenacity ring in my ears. My beloved mother Haixia passed away while I was pursuing my Ph.D. degree but her spirit and love have never left my side and are very special. May she rest in peace.

I also dedicate this dissertation to my wife Fei Cao who has supported me throughout the entire doctorate program. I will always appreciate all she has done and she is always my good life partner as well as a great friend. Her toughness and tenderness helped me to overcome difficulties in every aspect of my life. And I will always be there for her.

I dedicate this work and give special thanks to my advisor Dr. Carl W. Baum, for helping me develop my technical skills, for the many hours of advising and revising my writing.

Acknowledgements

I wish to thank my committee members who were more than generous with their expertise and precious time. A special thanks to Dr. Carl W. Baum, my committee chairman for his countless hours of reflecting, reading, encouraging, and most of all patience throughout the entire process. Thank you, Dr. Harlan B. Russell, Dr. Robert J. Schalkoff, Dr. Yue Wang for agreeing to serve on my committee.

I would like to acknowledge and thank my department for allowing me to conduct my research and providing any assistance requested. Special thanks to Dr. John N. Gowdy for his advice and encouragement.

Contents

List of Figures

Chapter 1

Introduction

Detecting and mitigating nuclear threats in metropolitan areas has drawn great attention in the past decade. Nuclear contamination from conventional nuclear devices and "dirty bombs" have the potential to severely disrupt our way of life. Nuclear sources can be obtained from research materials, medical waste, and many other sources. To mitigate the threat of terrorists causing nuclear contamination, robust nuclear detection systems must be developed for populous metropolitan areas. By using a pervasive surveillance and proactive monitoring system, one can provide constant detection and protection to such areas.

Localization of nuclear materials presents a wide variety of challenges. Because radiation from a nuclear source is probabilistic in nature, sources are appropriately modeled via Poisson processes [1]. However, if there is mobility in either the source or the detector, or (in some cases) if there is mobility of materials between the source and detector, the parameters of the Poisson process will vary over time, resulting in an inhomogeneous Poisson process.

A common approach to incorporating the effects of mobility in nuclear detection is to resort to detailed simulations [2], [3]. However, a simple model for the effects of the relative speed and distance between source and sensor is quite valuable, because it can both provide fundamental insight into the effects of mobility on detection and permit the development of low-complexity simulations that employ multiple simultaneous mobile sensors and/or

sources that are more realistic than simply assuming that detection is assured if a sensor comes within a certain distance of a source [4], [5]. In this work, we derive and present such a model. The analysis approach presented is applied to a variety of situations in which a single detector moves continuously in a field of operations in which a fixed source is present. The model can be readily expanded to account for mobility of the source, multiple sources, and multiple sensors; however, these extensions are beyond the scope of this work.

There have been a great number of studies regarding the coverage problem with sensor networks. Four main categories are studied based on physical approaches. The first type of network consists of static sensors only; the network is permanently deployed in an area and each sensor stays in the fixed location where it is assigned [4]-[11]. For such a network, the performance criterion is whether the area is "covered" by the sensors. The second type of network consists of dynamic sensors only and the sensors are all controlled [12]-[19]. Sensors are assigned specific paths; for these networks, computational cost is often the primary consideration. For both types of sensor networks, sensors must share information and should have the ability to perceive their locations. The third type of sensor network consists solely of uncontrolled sensors such as sensors attached to taxicabs. Here, the network exploits the random nature of the sensors' mobility to provide consistent monitoring [20]-[24]. For such networks, the deployment only occurs at the beginning of the detection task and the number of sensors in this type of sensor network is usually large. With no control over the sensors, same areas might be covered with multiple sensors while other areas remain unsensed. The final type of sensor network combines the second type and the third type and is called a hybrid mobile sensor network [25]-[32]. Here, controlled and uncontrolled sensors are deployed; the uncontrolled sensors provide a degree of coverage and controlled sensors are sent to explore the areas that have not been attended for a long period of time. This type of sensor network requires that the sensors communicate with a central controller that adaptively sends out sensors as conditions change. In this work, we focus on the hybrid mobile sensor network framework.

For hybrid mobile sensor networks, algorithms are proposed based on varying criteria

to evaluate the performance of the sensor network [25]-[32]. Most of the studies in this area focus on path-planning strategies. The basic idea in [28], [29] is to find the gaps in the grid map and send the mobile sensors to cover the gaps. Path-planning strategies typically take consideration of the energy consumption by the movement of the sensors. One common method widely applied is the virtual force method [26], which is a variation algorithm derived from artificial potential fields and potential functions [25], [31]. In this approach, each sensor is considered to be a virtual particle that is subject to virtual forces. The forces serve two functions: repulsive forces repel sensors from each other so as to spread out the sensors to maximize the coverage of the entire area, and attractive forces serve to guide the sensors' movement and eventually lead the network to reach equilibrium. Under these two types of forces, a mobile sensor network can automatically reconfigure itself due to any change in the target area. A concern of this method is that sensors move only when it is necessary to do so. By saving some energy, the surveillance result is worse because the inactive periods cause the mobile sensor network to be mostly static. Another probabilistic, non-heuristic method involves the use of a particle filter estimator algorithm which uses mutual information to plan the path of mobile sensors [30], [32]. The mutual information between the sensors and the target area is computed using a particle filter representation of the posterior probability distribution. There are two categories of computation; the first is to use particle filter estimators to compute the target area, and this method applies to the multimodal posterior distributions and nonlinear and non-Gaussian sensor models. The second approach is to use particle filters to estimate each sensor's position so as to improve the sensing capabilities of the network. The main weakness of the particle filter estimator method is its high computational cost. As for the surveillance of specifically nuclear materials in metropolitan areas, the Rutgers University group utilizes mobile sensor networks and vehicles' random movement [23], [24]. Using a latent modeling approach and likelihood inference to detect multiple spatial clusters, this method detects multiple clusters simultaneously in the entire region and filters out the potential nuclear source locations.

Based on these previous studies, we have conducted work on using hybrid mobile net-

works for surveillance as follows. We model detection as "on-off" in the sense that detection occurs with probability one if the distance between a sensor and the source ever drops below a fixed threshold. Detection occurs with probability zero otherwise. Each sensor (detector) installed on a vehicle reports to the central surveillance center whether the certain area has a source or not. At each time unit, the sensor only reports the area as "covered" to the central surveillance center if the area is inside the sensing range of the detector. We also model detection more accurately by using our probabilistic model already described. We note that this model can be used not only to evaluate system performance but also to design better surveillance models, and the design and analysis of such systems is an important part of this work.

Our network has two types of mobile sensors. The first type are random sensors such as taxicabs and public buses; let J denote the number of these sensors. Their movements are merely based on the demand of customers and are not controlled by the central surveillance center. The mobility of these sensors provides a degree of coverage in the entire metropolitan area. Typically the sensors installed on these vehicles are low-cost, medium range sensors. The second type of sensor is a controlled sensor; their movements are controlled by the central surveillance center and the number of this type of sensor is K, which is assumed to be relatively small compared to J. The algorithms used in this dissertation utilize a global assignment strategy. The metropolitan areas are divided into equal-area sub-regions, and each sub-region is further divided into smaller blocks. Once a vehicle (random or controlled) passes through the block and discovers no radiation, the location and time index information are sent to the central surveillance center. If radiation is discovered, action is required to further identify the source (but this is beyond the focus of our work). Our algorithms differ from the virtual force method in the way that we exploit the dynamic aspect of the mobile sensor network. Instead of trying to achieve a stationary network configuration after the effect of repulsive and attractive forces, our configuration is accomplished by the continuous movement of all the mobile sensors.

We utilize a real-time coverage information array to perform the global assignment

strategy and to evaluate the effect of the mobile sensor network. The array contains, for each block, the time that has elapsed since its last surveillance visit by a mobile sensor. The array also contains the current location of all $J + K$ mobile sensors. Optionally, a second array is used to provide estimate of the probability of miss as a function of where the sensors have traveled and at what speed. To evaluate the performance of the surveillance network, we consider two criteria: the percentage of the area covered by search vehicles in the last T time units (time-based coverage) and an estimate of the percentage of the area covered by search vehicles in the last T time units that has a probability of miss less than α (time and-probability-based coverage). The main difference between our evaluation criteria and those in previous research is that we focus on the continuous surveillance of areas and our goal is to assure that as much of the area has been visited "recently" as possible. Using these evaluation criteria, we have explored the effects of different global assignment strategies on performance. We have also explored the use of sub-region assignments to controlled sensors. In addition we have explored different movement strategies for sending the controlled sensors to the target sub-regions, some based only on the time information, and other based on time and probability information. Both static algorithms (with a fixed number of controlled sensors) and dynamic algorithms (in which the number of controlled sensors varies with conditions) have been considered. The algorithms are capable of detecting multiple locations with nuclear radiation sources in metropolitan areas.

The remainder of the dissertation is organized as follows. In Chapter 2, we explore the analysis of mobile detection of a stationary nuclear source. Chapter 3 considers the design and deployment of mobile sensor networks for monitoring nuclear radiation in metropolitan areas. Detection of specific locations in metropolitan areas with probability-based algorithms is analyzed in Chapter 4. Conclusions and future work are given in Chapter 5.

Chapter 2

Analysis of Mobile Detection of a Stationary Nuclear Source

In this chapter we present an analysis of the probability of detection of a stationary mobile source by a continuously moving detector. The remainder of this chapter is organized as follows. In Section 2.1, the general model and analysis approach is presented, and in Section 2.2, important definitions and properties of relevant functions are given. In Section 2.3, performance analysis is determined for a nuclear detector moving along an infinite linear path passing near a fixed nuclear source. In Section 2.4, a similar analysis is performed for the situation in which the mobile detector moves along a circular path. In Section 2.5, a rectangular path is analyzed, and in Section 2.6, three-dimensional generalizations of these results are obtained. Bayesian performance is considered in Section 2.7, and conclusions on the work are given in Section 2.8.

2.1 Modeling and General Analysis Approach

Consider a nuclear source in three-dimensional space at location (x_0, y_0, z_0) and source intensity λ_0. Assume a detector is in location $(x(t), y(t), z(t))$ at time t, so that the distance

$d(t)$ between source and detector at time t is given by

$$d(t) = \sqrt{(x(t) - x_0)^2 + (y(t) - y_0)^2 + (z(t) - z_0)^2}. \tag{2.1}$$

Define μ to be the photo-peak efficiency of the detector, and assume that this efficiency incorporates any branching factor that arises for the photo-peaks of whatever isotopes are involved in detection. Furthermore, define A to be the detector cross-sectional area, and assume that the detector obeys an efficiency proportional to the inverse square of the distance $d(t)$. Also define the air attenuation coefficient as ρ, the attenuation coefficient due to shielding (or any other non-air attenuation) as σ, and the corresponding thickness of shielding as d_s. If the background radiation at the detector is modeled as spatially uniform with rate λ_B, the incident count rate is given by

$$\lambda(t) = \lambda_B + \frac{\mu A \lambda_0}{4\pi d^2(t)} e^{-(\rho d(t) + \sigma d_s)}. \tag{2.2}$$

The effects of the source at our mobile detector is then modeled as a inhomogeneous Poisson process with rate $(\lambda(t))$.

This equation assumes that the detector cross-sectional area does not change as a function of the relative positions of source and sensor; that is, it assumes the detector is omnidirectional. The equation also assumes that attenuation due to materials other than air (e.g., shielding) does not change significantly as a function of the relative positions of source and sensor. It is possible to generalize the analysis for nonuniform shielding, but this topic is beyond the scope of this work.

To simplify the analysis, we assume that the background radiation is negligible compared to the radiation levels at the closer parts of the path traveled by the sensor. This permits us to focus on the probability of miss P_M as the key measure of performance. For the purposes of this analysis, we assume a miss occurs if no nuclear particles are detected. Although the effects of background radiation are important, in practice a Neyman-Pearson detection approach is used and false alarm thresholds are set such that the false alarm rate

is below an acceptable threshold. Our analysis exploits the complete lack of false alarms to obtain simple analytical results otherwise unobtainable. Importantly, these results allow us to explore the trade-offs between the effects of source intensity, velocity, path, and other variables. The qualitative behavior of these trade-offs are unlikely to change in a system with background radiation.

To simplify notation, we define

$$C = \frac{\mu A \lambda_0}{4\pi} e^{-\sigma d_s} \tag{2.3}$$

so that $\lambda(t)$ can be written as

$$\lambda(t) = \frac{C}{d^2(t)} e^{-\rho d(t)}. \tag{2.4}$$

Our approach is to use a discretized model of the detector and then use a limiting argument to evaluate the actual situation. Assume the detector spends time t_0 at a position at distance $d(kt_0)$ from the source. The detector then jumps immediately to a new position at distance $d((k+1)t_0)$ and continues to jump every t_0 seconds. For notational simplicity we assume that the distance $d(0)$ occurs at a time slot starting at time $t = 0$.

Let N_k denote the number of particles detected over the kth such time slot. It follows that N_k is Poisson with parameter $\frac{Ct_0}{d^2(kt_0)} e^{-\rho d(kt_0)}$. Because a Poisson process has independent increments, it also follows that the N_ks are mutually independent.

The probability of a miss for the discretized model is therefore given by

$$P_M = \prod_{k=-\infty}^{\infty} P(N_k = 0). \tag{2.5}$$

The Poisson model implies that

$$P(N_k = 0) = \exp(-\tfrac{Ct_0}{d^2(kt_0)} e^{-\rho d(kt_0)}) \tag{2.6}$$

which gives

$$P_M = \exp(-\sum_{k=-\infty}^{\infty} -\frac{Ct_0}{d^2(kt_0)} e^{-\rho d(kt_0)}) \tag{2.7}$$

To remove the effects of discretization, consider the limit

$$L = \lim_{t_0 \to 0} \sum_{k=-\infty}^{\infty} \frac{Ct_0}{d^2(kt_0)} e^{-\rho d(kt_0)}. \tag{2.8}$$

In the limit the summation becomes an integral. Specifically, t_0 is replaced by the differential element dt and kt_0 is replaced by t. The result is

$$L = \int_{-\infty}^{\infty} \frac{C}{d^2(t)} e^{-\rho d(t)} dt. \tag{2.9}$$

It follows that

$$P_M = \exp\left(-\int_{-\infty}^{\infty} \frac{C}{d^2(t)} e^{-\rho d(t)} dt\right). \tag{2.10}$$

This equation can be evaluated for a variety of mobility models of interest.

2.2 Special Functions

As (2.10) is evaluated for special cases, it will be seen that certain integral functions arise. In this section we present these functions along with useful properties of these functions.

The first function is a function of one variable. Denoted $R(a)$, this function is defined as

$$R(a) = \frac{1}{\pi} \int_{-\pi/2}^{\pi/2} e^{-a \sec(u)} du. \tag{2.11}$$

This function has the properties that $R(0) = 1$ and $R(a) \leq e^{-a}$ for all $a \geq 0$. It can be shown that $R(a)$ decreases from 1 to 0 as a increases from 0 to infinity.

The second function is a function of two variables. Denoted $R(a, b)$, this function is defined as

$$R(a, b) = \frac{1}{\pi} \int_{-\pi/2}^{\pi/2} e^{-a \sec(u)/\sqrt{1+b \tan^2(u)}} du. \tag{2.12}$$

Note that this function only exists if $b \geq 0$. Also note that $R(a,0) = R(a)$, $R(0,b) = 1$, and $R(a,1) = e^{-a}$. In addition, for $a \geq 0$, $R(a,b) \leq R(a)$ with equality only if $b = 0$.

We can, without loss of generality, restrict b to $0 \leq b \leq 1$, because a change of variables shows that $R(a,b) = R(\frac{a}{\sqrt{b}}, \frac{1}{b})$. It follows that, if $b < 1$, $R(a,b) \leq R(\frac{a}{\sqrt{b}})$ is a tighter upper bound than $R(a,b) \leq R(a)$.

It can be shown that, for b held constant, $R(a,b)$ decreases from 1 to 0 as a increases from 0 to infinity. In addition, for a held constant, $R(a,b)$ increases from $R(a)$ to e^{-a} as b increases from 0 to 1. Note that one implication of this result is that $R(a,b) \geq e^{-a}$ for $0 \leq b \leq 1$.

The third function we consider is an "incomplete" version of the first; it has the same integrand as $R(a)$, but integrates over a smaller region. The function is denoted as $R(a; c_1, c_2)$ and is defined

$$R(a; c_1, c_2) = \frac{1}{\pi} \int_{\arctan(c_1)}^{\arctan(c_2)} e^{-a \sec(u)} du. \tag{2.13}$$

Note that $R(0; c_1, c_2) = \frac{1}{\pi}(\arctan(c_2) - \arctan(c_1))$ and $R(a; c_1, c_2) \leq e^{-a} R(0; c_1, c_2)$ for all $a \geq 0$. Furthermore, for c_1 and c_2 fixed, $R(a; c_1, c_2)$ decreases from $R(0; c_1, c_2)$ to 0 as a increases from 0 to infinity.

In addition, we note that the integrand obtains its maximum value at $u = 0$. A consequence is that if $c_1 \leq 0$ and $c_2 \geq 0$ (so that the maximum value of the integrand is included in the integral), $R(a; c_1, c_2) \geq \frac{1}{\pi}(\arctan(c_2) - \arctan(c_1)) R(a)$. As a particular example of this inequality, we have $R(a; -1, 1) \geq \frac{1}{2} R(a)$.

2.3 Detection with a Sensor Moving Linearly

Consider a detection device moving linearly at constant speed v. Define ℓ to be the closest distance the detector ever comes to the source. The geometry of the situation is illustrated in Fig. 2.1. Without loss of generality, assume that the detection device achieves this minimum distance at time $t = 0$. The distance between the source and detector is at time t is $d(t) = \sqrt{\ell^2 + v^2 t^2}$.

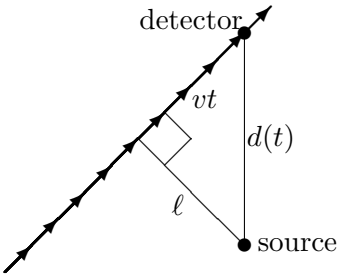

Figure 2.1: Fixed source and mobile detector moving linearly.

Applying this expression for $d(t)$ to (2.9), we have

$$L = \int_{-\infty}^{\infty} \tfrac{C}{\ell^2+v^2t^2} e^{-\rho\sqrt{\ell^2+v^2t^2}} dt. \tag{2.14}$$

Using the change of variables $t = \frac{\ell}{v}\tan(u)$ and the fact that $1 + \tan^2(u) = \sec^2(u)$ gives

$$L = \tfrac{C}{\ell v} \int_{-\pi/2}^{\pi/2} e^{-\rho\ell\sec(u)} du. \tag{2.15}$$

Using our definition of $R(a)$ in (2.11), we have

$$L = \tfrac{C\pi}{\ell v} R(\rho\ell), \tag{2.16}$$

and letting $P_M^L(\ell)$ denote the probability of miss for an infinite linear path at minimum distance ℓ from the source, applying (2.10) we obtain

$$P_M^L(\ell) = \exp(-\tfrac{C\pi}{\ell v} R(\rho\ell)). \tag{2.17}$$

Note that this expression depends on C (a factor proportional to the source strength λ_0) and v (the speed of the mobile detector) solely through their ratio. For this reason, Fig. 2.2 presents performance of the miss probability as a function of ℓ for four fixed values of C/v. For this and all subsequent plots we use the constant $\rho = 0.0097$ m^{-1} as the air attenuation coefficient. This value is based on the Cs-137 photo-peak region of 662 keV.

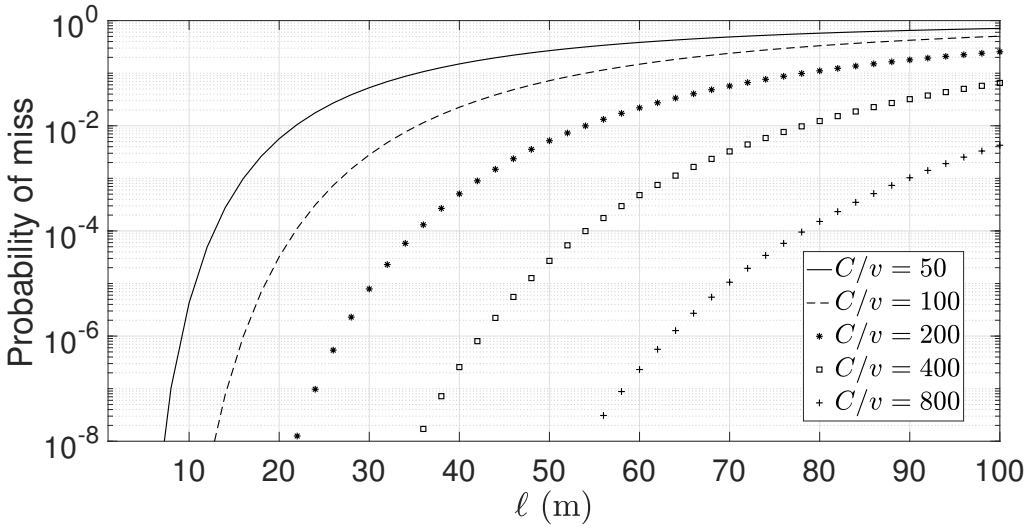

Figure 2.2: Probability of miss for detection with sensor moving linearly.

As expected the probability of miss increases as the distance between source and detector ℓ increases. Furthermore, the probability of miss decreases with increasing C or decreasing detector speed v. The behavior with respect to v is explained by noting that a slower speed permits a greater amount of time for detection when the detector is close to the source.

2.4 Detection with a Sensor Moving Circularly

Now consider a detection device moving in a circular path of radius r at constant speed v. Assume the circle is centered at the origin of an x-y plane, and assume the source is located (without loss of generality) at position $(x, 0)$, where $x \geq 0$. The geometry is illustrated in Fig. 2.3.

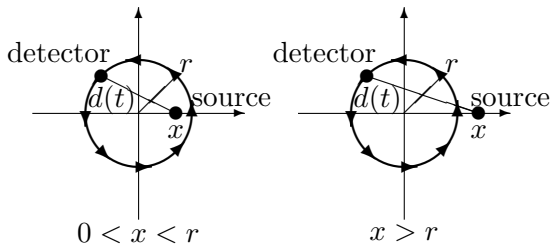

Figure 2.3: Fixed source and mobile detector moving circularly. Source is shown both interior and exterior to the path of the detector.

Further assume that the detector position at time t is given by the parametric equations $x(t) = r\cos(\frac{vt}{r})$ and $y(t) = r\sin(\frac{vt}{r})$, valid for $-\frac{\pi r}{v} \leq t < \frac{\pi r}{v}$. Over this time duration the detector makes one complete rotation. The distance between source and detector is given by

$$\begin{aligned} d(t) =& \sqrt{(x - r\cos(\tfrac{vt}{r}))^2 + (r\sin(\tfrac{vt}{r}))^2} \\ =& \sqrt{r^2 + x^2 - 2xr\cos(\tfrac{vt}{r})} \end{aligned} \tag{2.18}$$

Applying this expression for $d(t)$ to (2.9), we have

$$L = \int_{\frac{-\pi r}{v}}^{\frac{\pi r}{v}} e^{-\rho\sqrt{r^2+x^2-2xr\cos(\frac{vt}{r})}} \frac{Cdt}{r^2+x^2-2xr\cos(\frac{vt}{r})} \tag{2.19}$$

Using the change of variable $\theta = \frac{vt}{2r}$ gives

$$L = \int_{\frac{-\pi}{2}}^{\frac{\pi}{2}} e^{-\rho\sqrt{r^2+x^2-2xr\cos(2\theta)}} \frac{(2Cr/v)d\theta}{r^2+x^2-2xr\cos(2\theta)} \tag{2.20}$$

Applying the trigonometric identity $\cos(2\theta) = 2\cos^2(\theta) - 1$ gives

$$L = \int_{\frac{-\pi}{2}}^{\frac{\pi}{2}} e^{-\rho\sqrt{(r+x)^2-4xr\cos^2(\theta)}} \frac{(2Cr/v)d\theta}{(r+x)^2-4xr\cos^2(\theta)} \tag{2.21}$$

Using the change of variable $u = \arctan(\frac{r+x}{r-x}\tan\theta)$ further gives

$$L = \frac{2Cr/v}{|r^2-x^2|} \int_{-\pi/2}^{\pi/2} e^{-\rho|r-x|\sec(u)/\sqrt{1+(\frac{r-x}{r+x})^2\tan^2(u)}} du \tag{2.22}$$

Using our definition of $R(a,b)$ in (2.12), we obtain

$$L = \tfrac{2Cr\pi}{v|r^2-x^2|} R(\rho|r-x|, \tfrac{(r-x)^2}{(r+x)^2}). \tag{2.23}$$

Let $P_M^C(x,r)$ denote the probability of miss for a circular path of radius r centered at the origin and a source at a distance x from the origin. Applying (2.10), we obtain

$$P_M^C(x,r) = \exp(-\tfrac{2Cr\pi}{v|r^2-x^2|} R(\rho|r-x|, \tfrac{(r-x)^2}{(r+x)^2})). \tag{2.24}$$

Consider the special case in which the nuclear source lies in the exact center of the circular path. This case is highly unlikely to occur in practice, but it is of interest to explore how the equations simplify in this case. Here, we have $x = 0$, and because $R(a,1) = e^{-a}$,

(2.24) simplifies to the following:

$$P_M^C(0,r) = \exp(-\tfrac{2C\pi}{vr}e^{-\rho r}). \tag{2.25}$$

Because $R(a,b)$ decreases as a increases when b is held constant, and because $R(a,b) \geq e^{-a}$, we can write, for $0 \leq x \leq r$ (x inside the circle),

$$R(\rho|r-x|, \tfrac{(r-x)^2}{(r+x)^2}) \geq R(\rho r, \tfrac{(r-x)^2}{(r+x)^2}) \geq e^{-\rho r}. \tag{2.26}$$

It follows that, because $\frac{1}{|r^2-x^2|} \geq \frac{1}{r^2}$ for all $0 \leq x \leq r$,

$$\begin{aligned} P_M^C(x,r) &\leq \exp(-\tfrac{2Cr\pi}{v|r^2-x^2|}e^{-\rho r}) \\ &\leq \exp(-\tfrac{2C\pi}{vr}e^{-\rho r}) \\ &= P_M^C(0,r) \end{aligned} \tag{2.27}$$

Thus, if the source is within the circle, the largest miss probability occurs if the source is at the center.

Note that if the source is outside the circle (i.e., $x > r$) and we let $\ell = x - r$, we can apply (2.24) to write

$$P_M^C(\ell + r, r) = \exp(-\tfrac{2C\pi r}{v\ell(2r+\ell)}R(\rho\ell, \tfrac{\ell^2}{(2r+\ell)^2})). \tag{2.28}$$

Because $\frac{2r}{2r+\ell} \leq 1$ and $R(a,b) \leq R(a)$, we can write

$$\begin{aligned} P_M^C(\ell + r, r) &\geq \exp(-\tfrac{C\pi}{v\ell}R(\rho\ell, \tfrac{\ell^2}{(2r+\ell)^2})) \\ &\geq \exp(-\tfrac{C\pi}{v\ell}R(\rho\ell)) \\ &= P_M^L(\ell). \end{aligned} \tag{2.29}$$

Thus, if the source is outside a circle at a minimum distance ℓ away from the circle, perfor-

mance is worse than that of an infinite line at the same minimum distance.

As in the case of the infinite line, (2.24) depends on C and v solely through their ratio. Fig. 2.4 presents performance of the miss probability as a function of ℓ for four fixed values of C/v. In this figure, the radius of the path is set to be 50 m.

The figure presents results for the source both inside the circular path ($x < 50$) and outside the path ($x > 50$), where units are in meters. As expected, the probability of miss increases as x increases beyond 50 and as x decreases below 50. For $0 \leq y \leq 50$, performance for the source at $x = y$ is better than than that for the source at $x = 100 - y$, even though the minimum distance between path and source is $50 - y$ in both cases. (For example, compare the performance with $x = 10$ with that at $x = 90$.) This result can be explained by noting that when $x = y$, the distance between source and detector varies between $50 - y$ and $50 + y$, but when $x = 100 - y$, the distance varies between $50 - y$ and $150 + y$. (For example, when $x = 10$, the distance varies between 40 and 60, whereas when $x = 90$, the distance varies between 40 and 140.) Similarly to the linear case, the probability of miss improves as either C is increased or v is decreased.

2.5 Detection Along a Rectangular Path

Because a rectangular path consists of four straight line segments, we first determine the performance due to a single finite straight line segment. Consider a detector moving along a path on the x axis of length $b - a$ from $x = a$ to $x = b$ and suppose the source is at $(0, \ell)$. The situation is illustrated in Fig. 2.5.

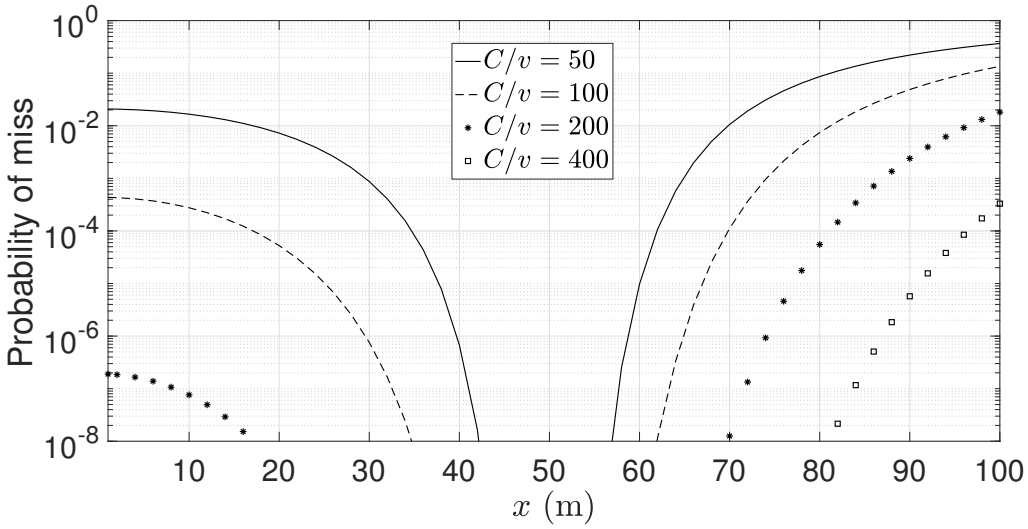

Figure 2.4: Probability of miss for detection with sensor moving circularly.

This problem is similar to that of Section 2.3 except that the length of the path is finite. Here $d(t) = \sqrt{\ell^2 + v^2t^2}$ from $t = \frac{r_1}{v}$ to $t = \frac{r_2}{v}$. Thus

$$L = \int_{r_1/v}^{r_2/v} \frac{C}{\ell^2 + v^2t^2} e^{-\rho\sqrt{\ell^2+v^2t^2}} dt. \tag{2.30}$$

Using the change of variables $t = \frac{\ell}{v}\tan(u)$ gives

$$L = \frac{C}{\ell v} \int_{\arctan(r_1/\ell)}^{\arctan(r_2/\ell)} e^{-\rho\ell\sec(u)} du, \tag{2.31}$$

and using (2.13) results in

$$L = \frac{C\pi}{\ell v} R(\rho\ell; \tfrac{r_1}{\ell}, \tfrac{r_2}{\ell}). \tag{2.32}$$

Let $P_M^L(\ell; r_1, r_2)$ denote the miss probability for this geometry. Applying (2.10) gives

$$P_M^L(\ell; r_1, r_2) = \exp(-\tfrac{C\pi}{\ell v} R(\rho\ell; \tfrac{r_1}{\ell}, \tfrac{r_2}{\ell})). \tag{2.33}$$

Now consider the situation of a rectangular path from $(0,0)$ to $(a,0)$ to (a,b) to $(0,b)$ back to $(0,0)$ with the source at (x,y). The source can be inside or outside the rectangle. Without loss of generality we assume $x > 0$ and $y > 0$. The situation is illustrated in Fig. 2.6.

The overall probability of miss is equal to the product of the four individual miss probability results for the four links. Denoting the overall probability of miss for the rectangle

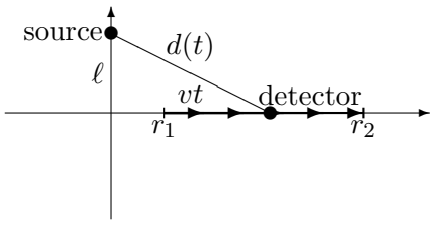

Figure 2.5: Fixed source and mobile detector moving over a straight line segment.

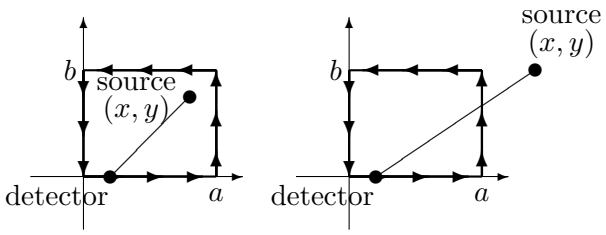

Figure 2.6: Fixed source and mobile detector moving along a rectangular path. Source is shown both interior and exterior to the path of the detector.

by $P_M^R(x, y; a, b)$, we have

$$\begin{aligned} P_M^R(x, y; a, b) = {} & P_M^L(y; -x, a - x) \\ & \times P_M^L(|a - x|; -y, b - y) \\ & \times P_M^L(|b - y|; -x, a - x) \\ & \times P_M^L(x; -y, b - y). \end{aligned} \tag{2.34}$$

where the first term is due to the bottom segment, the second is due to the right side, the third is due to the top segment, and the fourth is due to the left side.

Consider the special case that the source is in the center of a 2ℓ by 2ℓ square. In this case the results become

$$\begin{aligned} P_M^R(\ell, \ell; 2\ell, 2\ell) &= [P_M^L(\ell; -\ell, \ell)]^4 \\ &= \exp(-\tfrac{4C\pi}{\ell v} R(\rho\ell; -1, 1)) \end{aligned} \tag{2.35}$$

We compare this result with that for a source in the center of a circle with radius ℓ (so that the minimum distance from the path to the source is ℓ in both cases). Using the fact that $R(a; -1, 1) \leq \frac{1}{2} R(a)$, we have

$$P_M^R(\ell, \ell; 2\ell, 2\ell) \geq \exp(-\tfrac{2C\pi}{\ell v} R(\rho\ell)) = P_M^C(0, \ell). \tag{2.36}$$

Thus, at the same speed v, the smaller circular path has a smaller probability of miss than the square path. This result is not necessarily obvious; although the circular path remains closer to the source, the rectangular path, being longer, provides more *time* to collect data. The result shows that the benefits of the closer path outweigh the costs of a shorter collection time.

Fig. 2.7 presents performance for a square 100 m by 100 m path with coordinates $(0, 0)$, $(0, 100)$, $(100, 0)$ and $(100, 100)$ as a function of the parameter d. The coordinates of the source are $(d, 75)$ so that the locations lie on a horizontal line three-quarters of the way up on the square. Locations inside the square ($d < 100$) and locations outside the square ($d > 100$) are both considered. The results show behavior similar to that of the circular path. Performance is generally better than that of Fig. 2.4 because the minimum distance between source and detector in the rectangular case is smaller than that of the circular case (because the source is at location $(d, 75)$ in the rectangular case).

2.6 Paths in Three Dimensions

The analysis presented can be readily generalized for three dimensions. The results for linear paths apply without modifications provided ℓ is still the minimum distance between the path and the nuclear source. (That is, a two-dimensional coordinate system can always be constructed containing the line and the source point; in this coordinate system, the earlier results still apply.)

With regards to a circular path, the problem is fundamentally three-dimensional and requires modification of earlier results. Suppose the source is assumed to be at height h relative to the plane of the path. Then, otherwise using the same geometry as that of Fig. 2.3, the distance is given by

$$\begin{aligned} d(t) =& \sqrt{(x - r\cos(\tfrac{vt}{r}))^2 + (r\sin(\tfrac{vt}{r}))^2 + h^2} \\ =& \sqrt{r^2 + x^2 + h^2 - 2xr\cos(\tfrac{vt}{r})} \end{aligned} \tag{2.37}$$

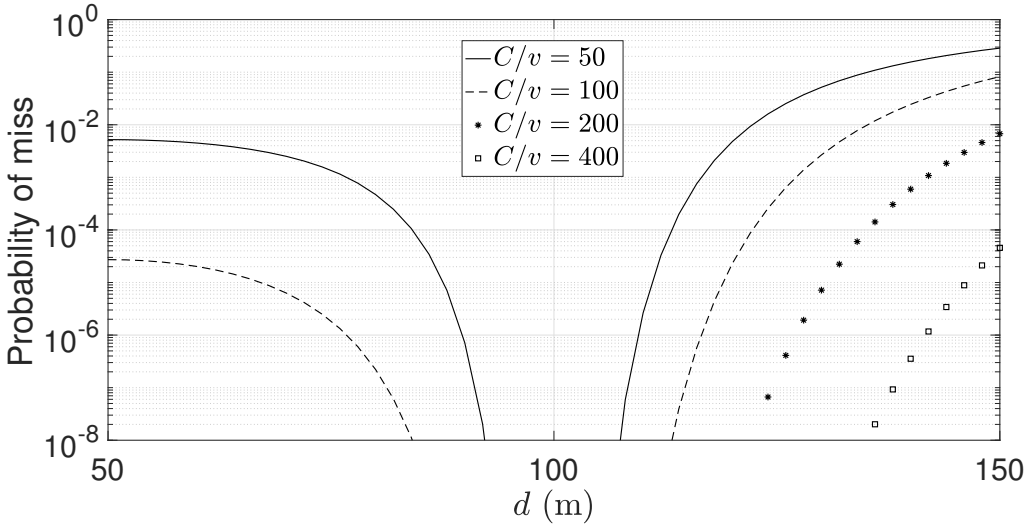

Figure 2.7: Probability of miss for detection along a rectangular path.

Using this expression in (2.9), performing the substitution $\theta = \frac{vt}{2r}$, using $\cos(2\theta) = 2\cos^2(\theta) - 1$, performing the substitution $u = \arctan(\sqrt{\frac{(r+x)^2+h^2}{(r-x)^2+h^2}}\tan(\theta)$, and finally using the definition of $R(a,b)$ in (2.12) gives

$$P_M^C(x,r,h) = \exp(-\frac{2\pi Cr/v}{\sqrt{[(r+x)^2+h^2][(r-x)^2+h^2]}} \times R(\rho\sqrt{(r-x)^2+h^2}, \frac{(r-x)^2+h^2}{(r+x)^2+h^2})). \tag{2.38}$$

As for the rectangular path, again assume the source is at height h relative to the plane of the path. Using the same geometry as that of Fig. 2.6,

$$\begin{aligned} P_M^R(x,y,h;a,b) = {} & P_M^L(\sqrt{y^2+h^2}; -x, a-x) \\ & \times P_M^L(\sqrt{(a-x)^2+h^2}; -y, b-y) \\ & \times P_M^L(\sqrt{(b-y)^2+h^2}; -x, a-x) \\ & \times P_M^L(\sqrt{x^2+h^2}; -y, b-y). \end{aligned} \tag{2.39}$$

where $P_M^L(\ell; r_1, r_2)$ is as defined in (2.33).

For the special cases that the source is at height h relative to the center of an 2ℓ by 2ℓ square and the center of a radius r circle, the results simplify to

$$\begin{aligned} & P_M^R(\ell,\ell,h;2\ell,2\ell) \\ & \quad = [P_M^L(\sqrt{\ell^2+h^2}; -\ell, \ell)]^4 \\ & \quad = \exp(-\tfrac{4C\pi}{v\sqrt{\ell^2+h^2}} R(\rho\sqrt{\ell^2+h^2}; \tfrac{-\ell}{\sqrt{\ell^2+h^2}}, \tfrac{\ell}{\sqrt{\ell^2+h^2}}) \end{aligned} \tag{2.40}$$

and

$$\begin{aligned} P_M^C(0,r,h) &= \exp(-\tfrac{2\pi Cr}{v(r^2+h^2)} R(\rho\sqrt{r^2+h^2}, 1)) \\ &= \exp(-\tfrac{2\pi Cr}{v(r^2+h^2)} e^{-\rho\sqrt{r^2+h^2}}) \end{aligned} \tag{2.41}$$

In practice the source is unlikely to be in the exact center of the search path. However, these special-case equations demonstrate some interesting behavior that also occurs in the more general situation. Perhaps surprisingly, for fixed values of h, performance is a non-monotonic function of ℓ (or r). Specifically, once h is set, there is in each case an optimum value of ℓ (or r) that minimizes the probability of miss. The trade-off here is due to the fact that although a larger value of ℓ (or r) results in a path further away from the source, it also provides a longer data accumulation time. It is straightforward to show that this optimum value does not depend on the value of C/v.

Fig. 2.8 presents this performance for the circular path at five combinations of values of h. The nonmonotonicity of performance as a function of r is clearly shown. The optimal path radius grows with increasing h, and in fact, the optimal value of r is slightly less than h in each case.

2.7 Bayesian Performance

One approach to the practical use of the results presented is to evaluate at/design for worst cases, generally as far from the closest the search path gets to the source as possible. An alternative is to take a Bayesian approach and assign an *a priori* probability density to the location of the source. This latter approach is the focus of this section.

Reconsider the infinite straight line path and model the *a priori* density of the distance to the source L as $f_L(\ell)$. Then the *average* probability of miss is given by

$$\begin{aligned} P^L_{M,\text{avg}} &= \int_0^\infty f_L(\ell) P^L_M(\ell) d\ell \\ &= \int_0^\infty f_L(\ell) \exp(-\tfrac{C\pi}{\ell v} R(\rho\ell)) d\ell. \end{aligned} \tag{2.42}$$

Let μ denote the expected value of L and define $X = L/\mu$ so that $E[X] = 1$. Then

$$F_X(x) = P(X \le x) = P(L \le \mu x) = F_L(\mu x) \tag{2.43}$$

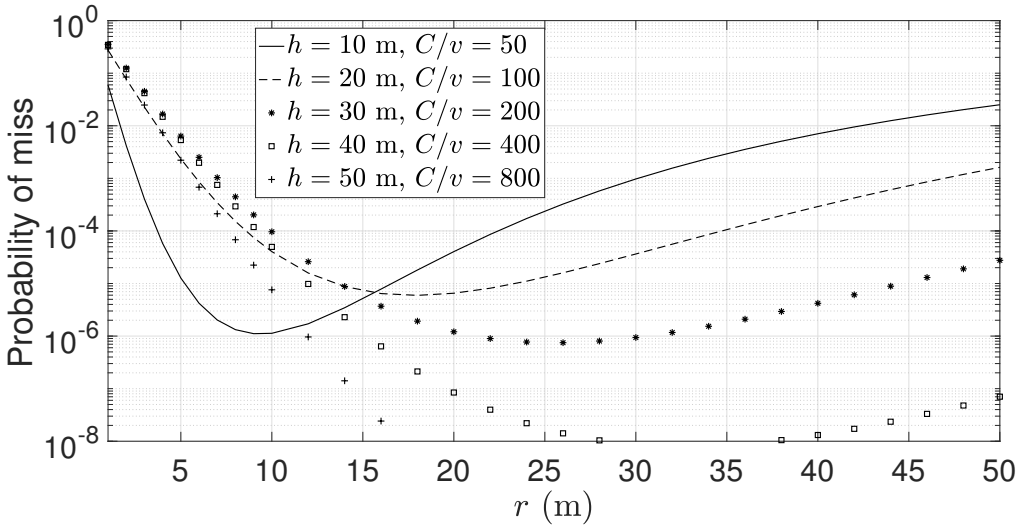

Figure 2.8: Probability of miss for detection in three dimensions.

and

$$f_X(x) = \frac{d}{dx} F_X(x) = \mu f_L(\mu x) \tag{2.44}$$

Performing the change of variable $x = \ell/\mu$ gives

$$P^L_{M,\text{avg}} = \int_0^\infty f_X(x) \exp(-\frac{C\pi}{x\mu v} R(\rho x \mu)) dx. \tag{2.45}$$

Possible models for X (required to have expected value equal to one) include uniform so that $f_X(x) = \frac{1}{2}$, $0 \le x \le 2$, triangular so that $f_X(x) = \frac{2}{3}(1 - \frac{x}{3})$, $0 \le x \le 3$, and exponential so that $f_X(x) = e^{-x}$, $x \ge 0$. The integral can be evaluated numerically in each case.

Fig. 2.9 presents a comparison of the three models as a function of C/v with $\overline{L} = 50$ m. The figure shows performance improves as C/v increases, as expected. However, the *rate* of improvement varies significantly depending on the Bayesian model of $f_X(x)$ used. Improvement increases at the greatest rate with the uniform model and at the smallest rate with the exponential model. These results can be explained by the fact that the uniform density has the smallest variance and the exponential density has the largest variance. The large variance of the exponential corresponds to a higher probability that the minimum distance between source and detector will be large.

As a second example of Bayesian modeling, reconsider the circular path of radius r and model the location of the source as uniformly distributed within a circle of radius s. Let L be a random variable denoting the distance of the source from the center. To achieve the uniform distribution in two-dimensional space, the probability of an area must equal the ratio of the area divided by the area of the circle. Thus, the distribution function for L must be

$$F_L(\ell) = P(L \le \ell) = \frac{\pi \ell^2}{\pi s^2} = \frac{\ell^2}{s^2} \tag{2.46}$$

from which it follows that the density is

$$f_L(\ell) = \frac{d}{d\ell} F_L(\ell) = \frac{2\ell}{s^2} \tag{2.47}$$

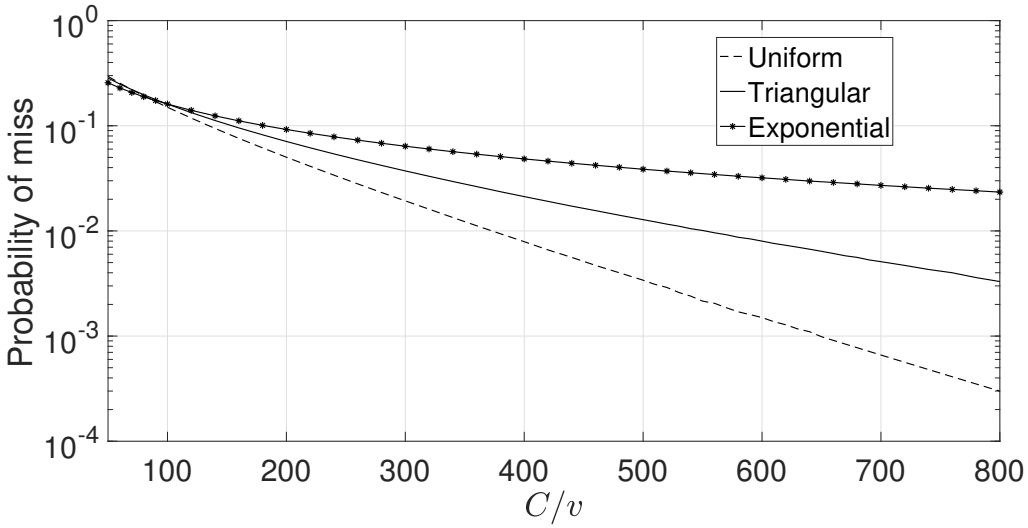

Figure 2.9: Probability of miss for detection with a sensor moving linearly.

valid for $0 \leq \ell \leq s$.

The average probability of miss is

$$P_{M,\text{avg}}^{C} = \int_0^s f_L(\ell) P_M^C(\ell, r) d\ell = \int_0^s \tfrac{2\ell}{s^2} P_M^C(\ell, r) d\ell \tag{2.48}$$

where $P_M^C(\ell, r)$ is given by (2.24).

Fig. 2.10 presents performance as a function of path radius r when s is fixed at 50 m. Performance can be seen to be a non-monotonic function of r. It can be seen that the optimal search radius is not around the periphery of the region in which the source is assumed to lie (which corresponds to $r = 50$ m); instead, the optimal search radius is smaller, one in which the source may lie inside or outside the path of the detector (around $r = 35$ m). The exact optimal value of r depends on C/v.

However, using $r = 35$ m gives near-optimal performance over a wide range of C/v values. Note that there is a large difference in performance between $r = 50$ and $r = 35$ m; for $C/v = 100$, the difference is roughly a factor of 100 (two orders of magnitude).

As an example of Bayesian analysis with three-dimensional modeling, suppose the detector takes a circular path of radius r on the ground, and the source lies uniformly within a cylinder of the same radius r and height h. Such a situation might model a ground-based search for nuclear material around a high-rise building. Here we obtain

$$P_{M,\text{avg}}^{C} = \int_0^r \int_0^h \tfrac{2\ell}{r^2 h} P_M^C(\ell, r, z) dz d\ell \tag{2.49}$$

where $P_M^C(\ell, r, z)$ is given by (2.38).

This equation can be used to explore what cylindrical building shape, for a fixed total volume, has the worst probability of miss. Suppose the volume is fixed to be the same as that of a building with radius 50 m and height 50 m. Fig. 2.11 presents performance in this situation as a function of the height h. The figure shows that the *best* performance occurs in a building of height roughly 30 m (and radius roughly 65 m). Performance degrades significantly in tall buildings (r small) and in short ones (r large), in the former case

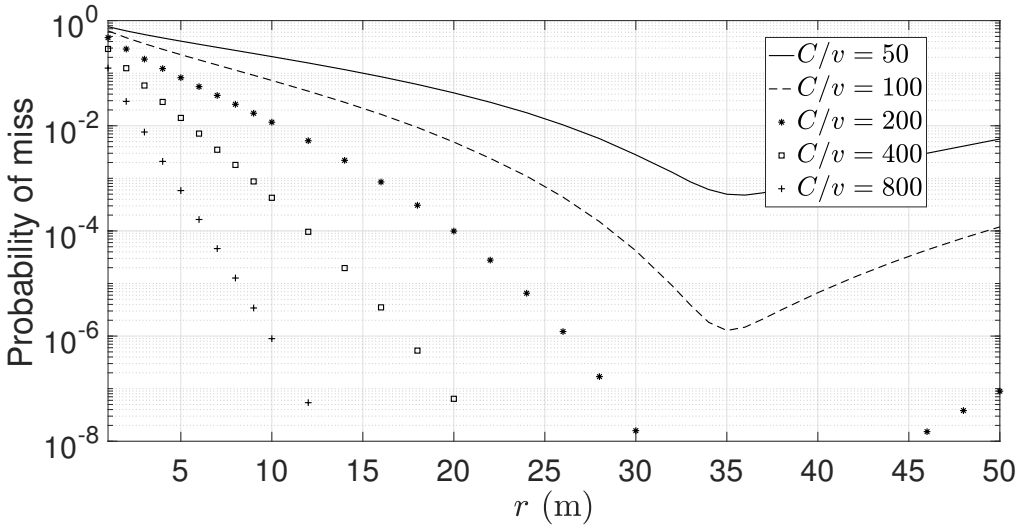

Figure 2.10: Probability of miss for detection with circular path.

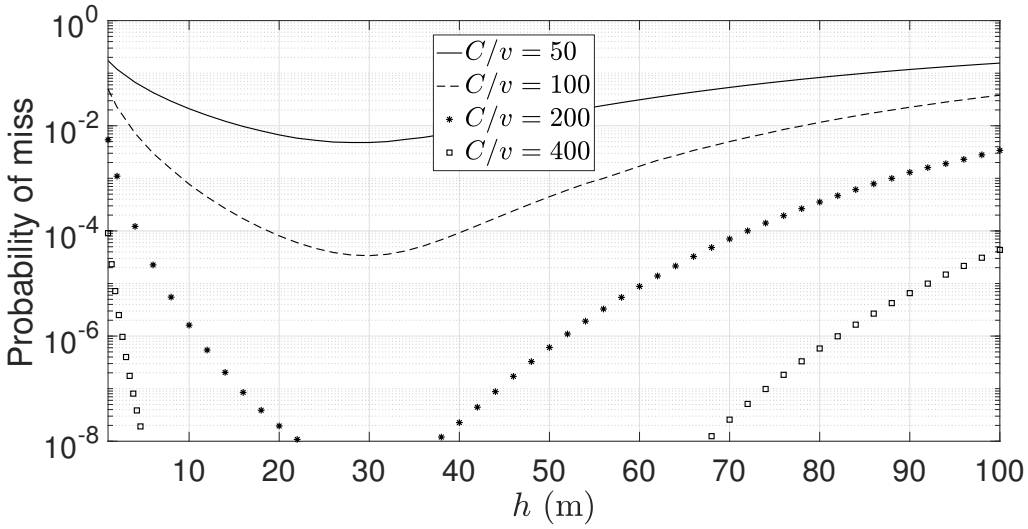

Figure 2.11: Probability of miss for detection of three-dimensional modeling.

because the source is likely to be far vertically from the ground and the search time is short, and in the latter case because the source is likely to be far horizontally from the detector path.

2.8 Conclusions

Expressions for the probability of detection of a nuclear source have been derived for a sensor that moves continuously. The analysis has been applied to linear and circular motion, and both two- and three-dimensional topologies have been analyzed. Generalizing the results for non-uniform shielding is a useful area of future research, as is incorporating the effects of non-negligible background radiation. However, we do not explore these topics in this dissertation.

Chapter 3

Design and Analysis of Mobile Sensor Networks for Surveillance of Metropolitan Areas

In this chapter we present results of hybrid surveillance sensor research using the "on-off" source detection model. This chapter is organized as follows: In Section 3.1, the hybrid surveillance sensor network model with sub-regions is proposed. Section 3.2 presents simulation results for a sensor network in a metropolitan area. Simulation results are compared with no global assignment and various movement strategies in Section 3.3. Also, the algorithm with dynamic number of controlled sensors are performed in Section 3.3. Conclusions are given in section 3.4.

3.1 Hybrid Surveillance of Mobile Sensor Network with Sub-regions

Consider a metropolitan area divided into equal-area sub-regions. Two types of sensors are considered in the hybrid surveillance model. A number of mobile vehicles (J) such as

taxicabs or public buses are equipped with detectors and Global Position Systems (GPS), and their movements are not controlled by the central surveillance center. These vehicles are viewed as uncontrolled sensors because we can not control their movements. The paths of uncontrolled sensors are determined by the passengers they take or by predefined routes; they may stay static when they do not carry any passengers. Uncontrolled sensors provide position data and a certain degree of coverage of a metropolitan area. A smaller number of mobile vehicles (K) such as police-cars or dedicated vehicles are also equipped with detectors and GPS and their movements are controlled by the central surveillance center. Taxicabs without passengers may also be hired for this purpose. These vehicles are viewed as controlled sensors. Each controlled sensor is assigned a sub-region and searches that sub-region until told to move to a different sub-region. The combination of uncontrolled sensors and controlled sensors defines the hybrid sensor network surveillance model.

Each sub-region is further divided into smaller blocks. For simulation purposes, assume all blocks are square with equal dimensions. After a vehicle (controlled or uncontrolled) passes through a block and discovers an absence of radiation, the location information and time index information are sent to the central surveillance center. If radiation is discovered, action is needed to further identify the location of the source, but subsequent actions and decisions are not the focus of this research. As a result of obtaining this information, the central surveillance center maintains a Real-Time Coverage Information Array at all times. The central surveillance center knows, for every block, the time that has elapsed since its last surveillance visit. The center also maintains the current locations of all $J + K$ vehicles.

3.1.1 Global Sub-region Assignment

With the metropolitan areas divided into sub-regions, time index information is used to determine which sub-region should be attended by a given controlled sensor. The criterion applied to determine whether the sub-region needs to be revisited is the Worst Time Information criterion, defined to be the longest time elapsed for a block since it has last been visited. Two methods are utilized to compute the worst time information for each sub-

region. The first we call the Worst Sum algorithm. Here, all blocks within the sub-region are considered. The sum of the time indexes of all blocks within the sub-region is used as the indicator of the sub-region. The second method we call the Worst Unit algorithm. In this case, only the block with the worst time index information in the sub-region is considered. The time index of the block with longest time elapsed since it has last been visited is used as the indicator of the sub-region in this case. With both of these methods, each sub-region is represented by a time index, and this index is used to identify the sub-region with the worst time index information in the entire metropolitan area. The unoccupied controlled sensor is assigned to this sub-region. This assignment procedure occurs asynchronously and is used to immediately deploy any inactive controlled sensor.

An example of an array containing the times since the last visit is shown in Fig. 3.1. Here A(i,j) is the time since the last visit in the ith row and jth column of sub-region A. The worst sum algorithm chooses as the next sub-region to visit the sub-region that corresponds to the largest value of $\sum_i \sum_j A(i,j)$, $\sum_i \sum_j B(i,j)$, ..., $\sum_i \sum_j I(i,j)$, and the Worst Unit algorithm chooses as the next sub-region the one that corresponds to the largest value of $\max_i \max_j A(i,j)$, $\max_i \max_j B(i,j)$, ..., $\max_i \max_j I(i,j)$.

A(1,1)	A(1,2)	A(1,3)	B(1,1)	B(1,2)	B(1,3)	C(1,1)	C(1,2)	C(1,3)
A(2,1)	A(2,2)	A(2,3)	B(2,1)	B(2,2)	B(2,3)	C(2,1)	C(2,2)	C(2,3)
A(3,1)	A(3,2)	A(3,3)	B(3,1)	B(3,2)	B(3,3)	C(3,1)	C(3,2)	C(3,3)
D(1,1)	D(1,2)	D(1,3)	E(1,1)	E(1,2)	E(1,3)	F(1,1)	F(1,2)	F(1,3)
D(2,1)	D(2,2)	D(2,3)	E(2,1)	E(2,2)	E(2,3)	F(2,1)	F(2,2)	F(2,3)
D(3,1)	D(3,2)	D(3,3)	E(3,1)	E(3,2)	E(3,3)	F(3,1)	F(3,2)	F(3,3)
G(1,1)	G(1,2)	G(1,3)	H(1,1)	H(1,2)	H(1,3)	I(1,1)	I(1,2)	I(1,3)
G(2,1)	G(2,2)	G(2,3)	H(2,1)	H(2,2)	H(2,3)	I(2,1)	I(2,2)	I(2,3)
G(3,1)	G(3,2)	G(3,3)	H(3,1)	H(3,2)	H(3,3)	I(3,1)	I(3,2)	I(3,3)

Figure 3.1: Array of times since last visit, incorporating sub-regions.

3.1.2 Surveillance within a Sub-region

Once a sub-region has been selected, the controlled sensor must go to that sub-region and provide surveillance. Four surveillance strategies have been considered in this research.

The first movement strategy is the most intuitive one, which we call the Sweeping Movement Strategy. Controlled sensors go through every block in the target sub-region and perform detection along an "S"-shape path. That is, the sensor traverses each row of blocks and goes to the next row when it finishes the current row, alternating directions with each row. The procedure can be generalized for non rectangular or otherwise irregular blocks, but the idea is to "sweep" methodically through the sub-region. The time spent by the controlled sensor in the sub-region is proportional to the area of the sub-region. In the case of equal square blocks, the controlled sensor revisits all blocks in the sub-region once and only once. Upon completion of surveillance in the sub-region, the controlled sensor is assigned to another sub-region via the global sub-region assignment method already described. An example of the path taken using the Sweeping Movement Strategy in a square area is shown in Fig. 3.2. This figure assumes that the controlled sensor enters the sub-region in the upper left corner.

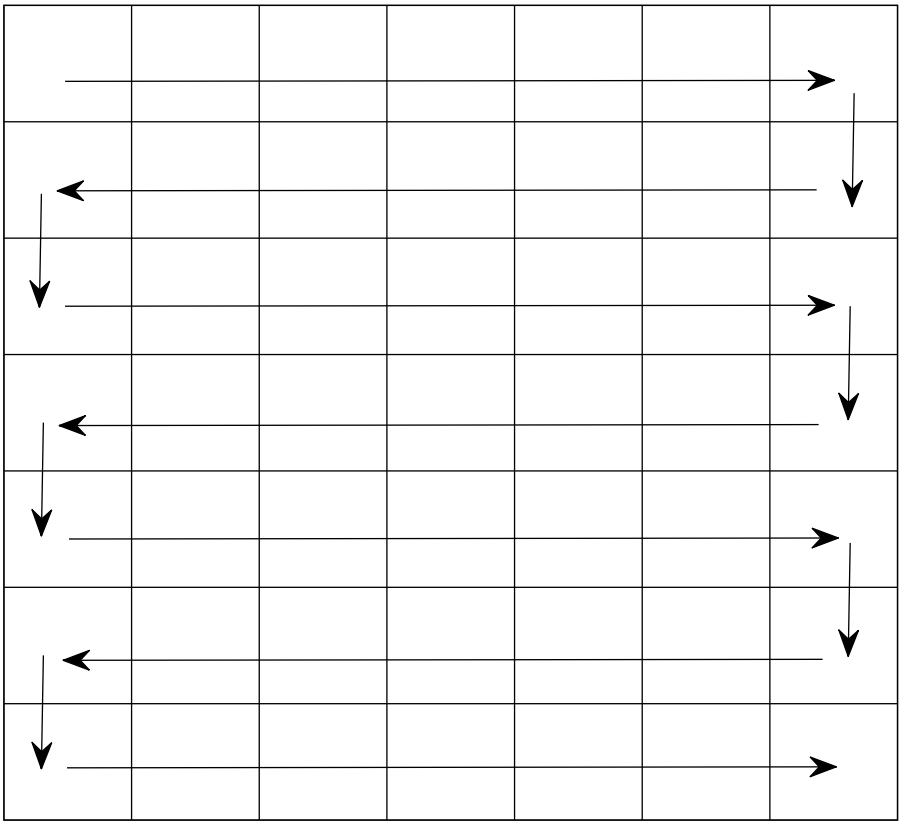

Figure 3.2: Sweeping movement strategy.

The remaining three movement strategies exploit the time index information in the neighborhood blocks and they are elaborated as follows. A one-step neighborhood consists of blocks within one block-distance away from the current block; two and three-step neighborhoods consist of all blocks within two or three block-distances away from the current block. An illustration of one, two and three-step neighborhoods is given in Fig. 3.3. One-step neighborhood, two-step neighborhood and three-step neighborhood time index information is used for one-step, two-step and three-step movement strategies. The worst time information is either the longest time elapsed in one block since it has last been visited (for a one-step neighborhood), or the largest sum of time elapsed in two or three blocks since they were last visited (for a two-step neighborhood or three-step neighborhood). The neighborhood regions for one-step, two-step and three-step methods are strictly based on Manhattan distance. These quantities are calculated for each block immediately neighboring the current position of the controlled sensor, and the sensor travels to the "worst" neighboring block. The controlled sensor remains in the sub-region until it covers a fixed percentage of the area in the sub-region.

			3			
		3	2	3		
	3	2	1	2	3	
3	2	1	0	1	2	3
	3	2	1	2	3	
		3	2	3		
			3			

Figure 3.3: Information for neighborhood movement strategies.

3.1.3 Traveling Between Sub-regions for Controlled Sensors

Once the unoccupied controlled sensor is assigned a sub-region, it drives to that sub-region. The transition path is set by choosing the nearest corner block of the new sub-region; the transition path is from the current position of the controlled sensor to that corner block. Between these two locations there are multiple paths of equal (shortest) length. The general idea of selecting the path is that controlled sensors can detect some long-neglected blocks along the way. Based on this idea, we use a worst pixel path, which is defined as the path that visits n blocks with the worst time index information, where n is a constant. (In our simulation, $n = 100$.)

3.2 Sensor Network Simulation

3.2.1 Parameters and Details of Implementation

In this simulation, the dimension of the metropolitan area is defined as N by N, so that the area is divided into N^2 grid blocks. The metropolitan area is divided into sub-regions with dimension m by m, so that the total number of sub-regions is L^2, where $N = Lm$. With the Sweeping Movement strategy, the time spent in a sub-region is m^2 (in units of block search detection times) and for one-step neighborhood, two-step neighborhood and three-step neighborhood movement strategies, the time spent in a sub-region is m^2 or less, depending on the fixed percentage of area that is covered in the sub-region before switching to another sub-region. For all sensors, we model the sensing range as exactly one block, meaning that a sensor can only detect a source in the block it is located.

In the simulation, one time unit equals one block search. At every time unit, when an uncontrolled sensor or a controlled sensor reaches a block, this block is marked as detected and the information stored for this block is the time elapsed since it has last been visited. Through the continual movement of all sensors, the time information stored for each block updates continually. In the simulation, we model the time for a sensor to move

to a neighboring block as a part of the time unit used to surveil a block.

3.2.2 Uncontrolled Sensor Detection Model

Uncontrolled sensors are transportation vehicles that perform transportation tasks while surveilling the metropolitan area. We model the uncontrolled sensors as also traveling one block per time unit. Uncontrolled sensors always choose a shortest path between the pick-up location and the destination. There is always a straight line LP connecting these two blocks. Our movement model is that an uncontrolled sensor always chooses the direction towards the destination along a Manhattan-distance-type path closet to LP.

Uncontrolled sensors also experience a time period of waiting for the next service. We model the waiting period between two services as a Poisson random variable, so that the probability for the waiting time between two services is

$$P(W = k) = \frac{e^{-\lambda k}(\lambda)^k}{k!}, k = 0, 1...$$

The random sensor is modeled as stationary during the waiting period, and the detector is modeled as providing constant surveillance of the block in which it waits.

3.2.3 Controlled Sensor Detection Model

The movement of a controlled sensor is completely determined by the central surveillance center. The controlled sensor moves one block per time unit, never halts and performs surveillance continuously.

3.2.4 Simulation Initialization and Sampling

Each sensor is initially positioned randomly in the entire metropolitan area. To avoid spurious effects of initialization, we only collect data after an initialization period. For the results presented here, the initialization period is 10,000 time units and we collect data for the time period from time unit 10,000 to time unit 50,000. The criterion used to evaluate

the performance of the sensor network is the percentage of area covered within the last T time units as a function of T. Our results present the average of 400 simulations.

3.3 Simulation and Performance of the Sensor Network

In this section, simulation results of a sensor network are presented. The dimension of the metropolitan area is set to $N = 400$, and the dimension of a sub-region is $m = 25$, 40 and 80. Thus the number of sub-regions is $L^2 = 256$, 100 and 25. The number of uncontrolled sensors is $J = 80$ and number of controlled sensors is $K = 16$. For the uncontrolled sensors, the parameter of the Poisson random variable used to model the waiting period is $\lambda = 2$.

3.3.1 Performance with Global Sub-region Assignment Algorithm

In Figs. 3.4 through 3.6, the effects of different sub-region assignment algorithms are presented. Fig. 3.4 presents results for 25 by 25 block sub-regions, Fig. 3.5 gives results for 40 by 40 block sub-regions, and Fig. 3.6 gives results for 80 by 80 block sub-region. Performance is measured via time unit 3,000 to time unit 7,500 for T, and the vertical axis shows the percentage of area covered within the last T time units. The Worst Sum assignment algorithm and the Worst Unit assignment algorithm are compared with $K = 16$ controlled sensors. The worst pixel path method is also employed. The figures show that the Worst Sum assignment algorithm significantly outperforms the Worst Unit assignment algorithm, regardless of the size of sub-regions. We note that the Worst Sum assignment algorithm incorporates more information available from the sub-region than the Worst Unit assignment algorithm, as the worst unit assignment algorithm focuses on the block with the worst time index information in the sub-region but omits the neighborhood information inside the sub-region. Based on these results, we focus on the Worst Sum assignment algorithm in the remaining figures.

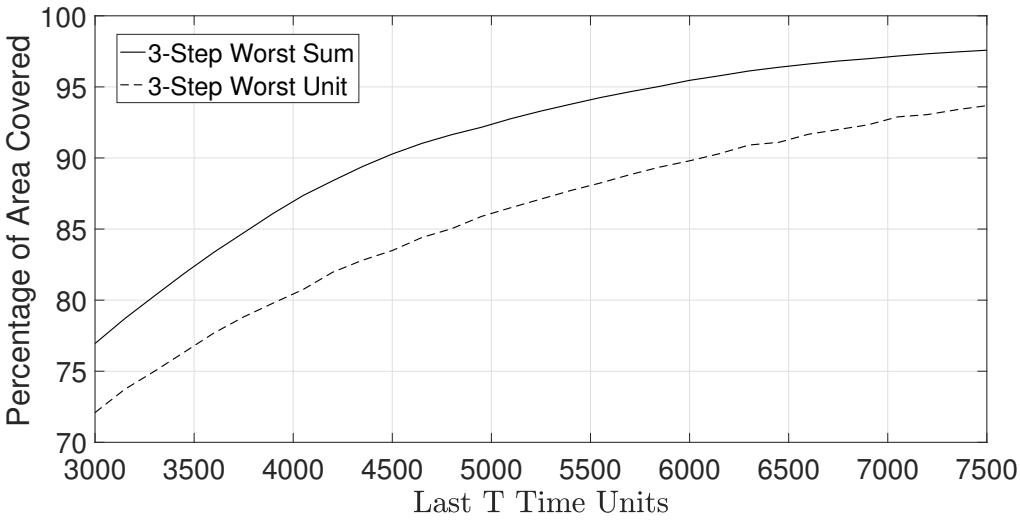

Figure 3.4: Percentage of area covered with the last T time units ($m = 25$).

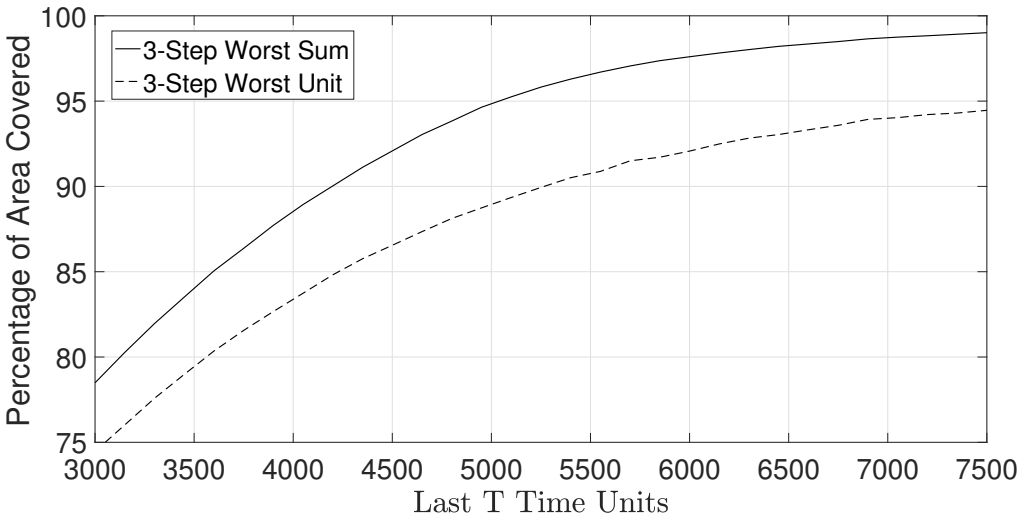

Figure 3.5: Percentage of area covered with the last T time units ($m = 40$).

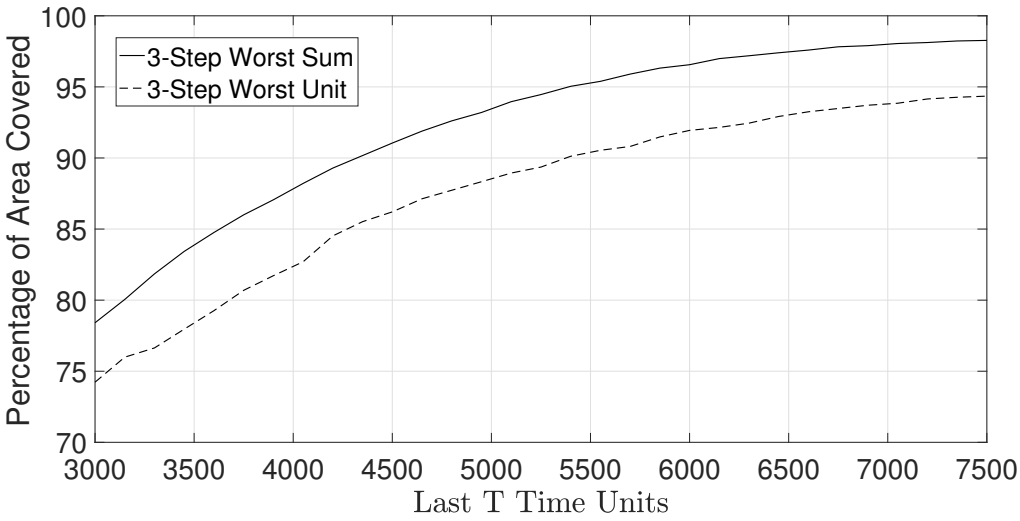

Figure 3.6: Percentage of area covered with the last T time units ($m = 80$).

3.3.2 Performance with Movement Strategies in a Sub-region

In this section, the four movement strategies are compared. We focus on the worst sum assignment algorithm and the worst pixel path for movement between sub-regions. For the one-step neighborhood, two-step neighborhood and three-step neighborhood movement strategies, we set the threshold for percentage of area covered within the last T time units as 99 percent of the sub-region. A controlled sensor therefore finishes the detection assignment when 99 percent of the sub-region is attended within the last T time units or when the controlled sensor remains in the sub-region for $m^2 = 625$, 1600 and 6400 time units, whichever occurs first. For comparison, we also consider the performance of a sensor network with no controlled sensors. To make the comparison fair, we add additional uncontrolled sensors so that the total number of sensors is the same in all cases. Results are shown in Figs. 3.7 through 3.9. The figures show that the three-step neighborhood movement strategy performs best. Regardless of sub-region size, the results show that the three-step neighborhood movement strategy outperforms the sweep approach and the two-step and one-step strategies, although in some cases the difference between the three-step strategy and the sweep approach is slight. The differences between the strategies is most pronounces using 80 by 80 block sub-regions. The results from all three figures also show that all hybrid strategies dramatically outperform a network with no controlled sensors.

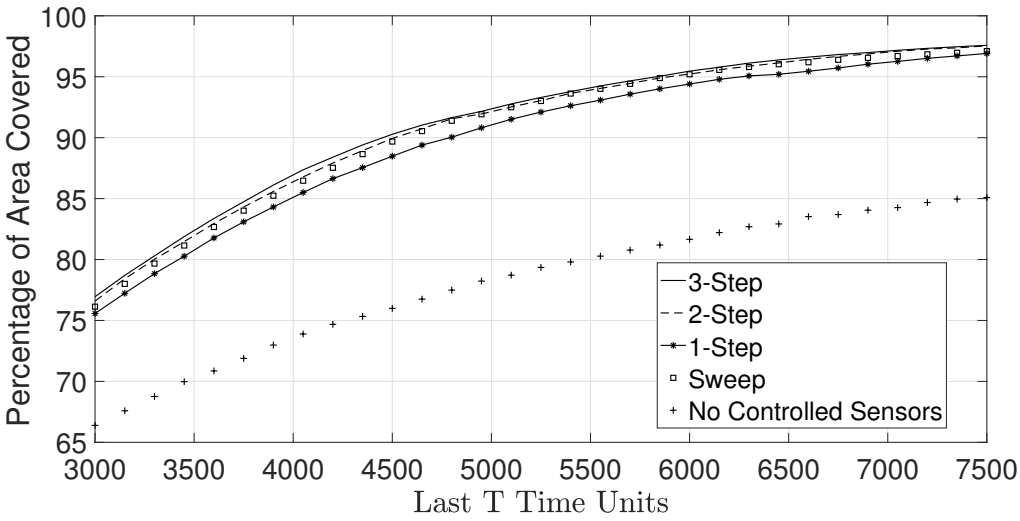

Figure 3.7: Percentage of area covered with the last T time units ($m = 25$).

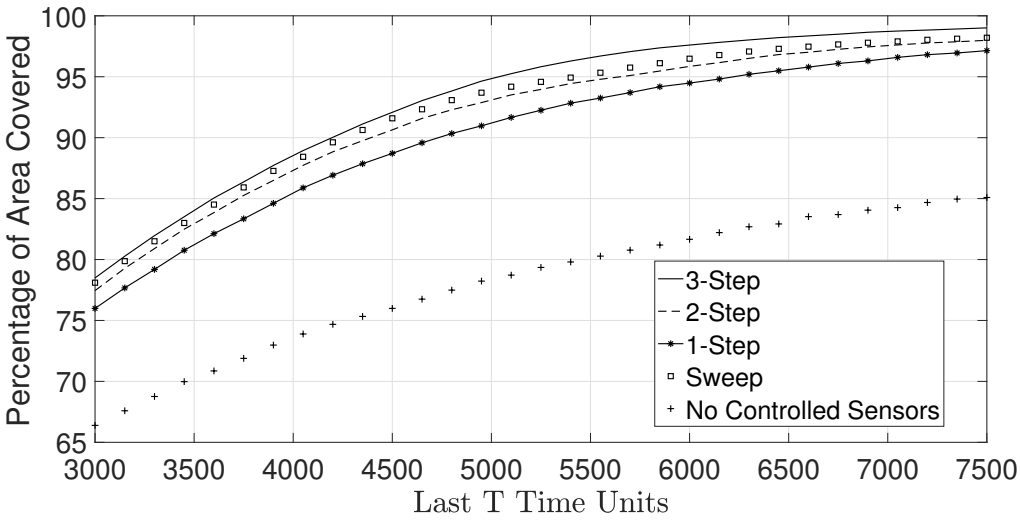

Figure 3.8: Percentage of area covered with the last T time units ($m = 40$).

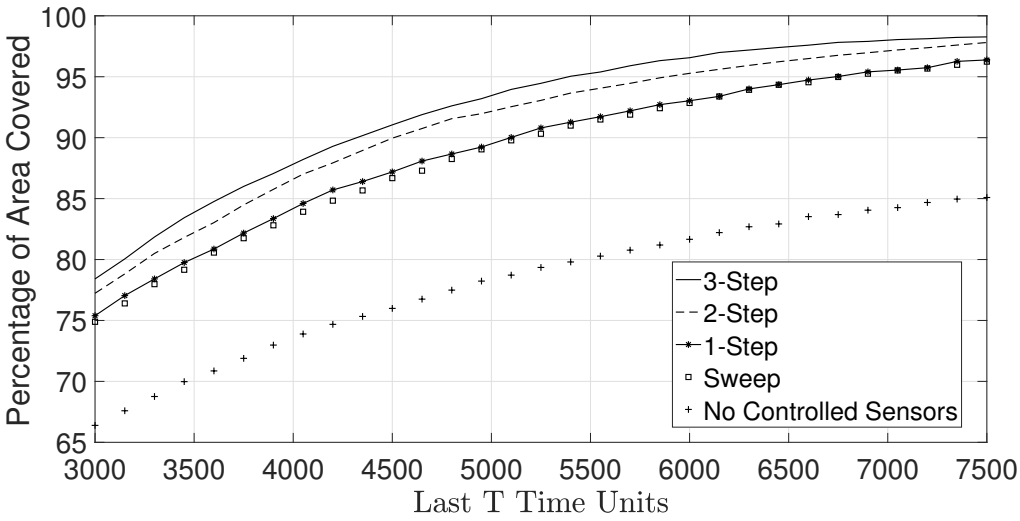

Figure 3.9: Percentage of area covered with the last T time units ($m = 80$).

3.3.3 Comparison of Global Assignment Algorithm and Local Assignment Algorithm

The global assignment algorithm has already been described. For comparison, consider the condition that one controlled sensor surveils each sub-region and confine the movement of a sensor to the sub-region initially assigned to it. For this local assignment algorithm, the number of sub-regions L equals the number of controlled sensors $K = 16$ in our case. The worst sum assignment algorithm and worst pixel path are applied with the global assignment algorithm, and the three-step neighborhood movement strategy is applied to both assignment algorithms. Simulation is performed with sub-region dimension $m = 40$.

Fig. 3.10 compares the performance of these assignment algorithms. It can be seen that the global assignment algorithm outperforms local assignment significantly. The advantage of the global assignment algorithm is that it sends sensors to the sub-regions in greatest need of surveillance. The results show that uncontrolled sensors are inadequate for providing uniform wide-area surveillance, even when assisted by controlled sensors with fixed assignments.

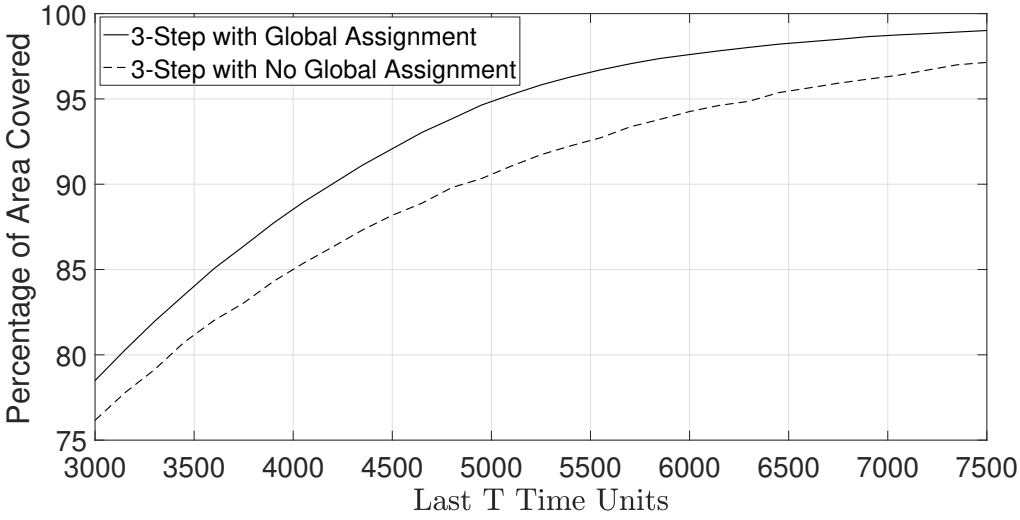

Figure 3.10: Percentage of area covered with the last T time units.

3.3.4 Performance of Sensor Network with the Changing Number of Controlled Sensors K

To better understand the performance of different movement strategies using the global assignment algorithm, we fix the dimension of sub-regions for each set of simulation and vary the number of controlled sensors K. Results are shown in Figs. 3.11 through 3.13 with $T = 5000$ for sub-regions with dimension 25 by 25, 40 by 40 and 80 by 80 blocks. All the previous movement strategies are considered and the worst pixel path algorithm is applied in each case. Results consistently show that the three-step strategy provides the best performance. The results show that the performance gap between the approaches increases as K increases. The results also show that although the sweep approach works reasonably well with 25 by 25 and 40 by 40 block sub-regions, it performs especially poorly when 80 by 80 block sub-regions are used.

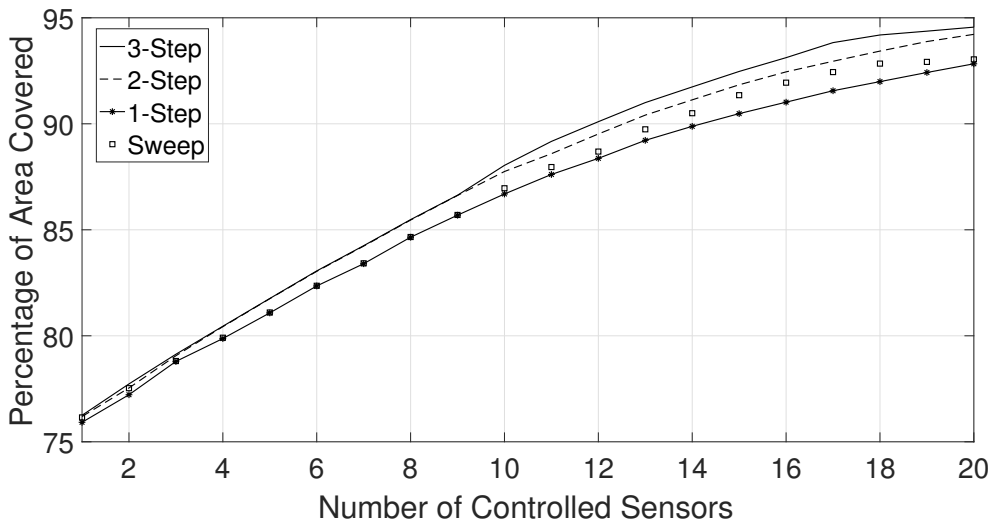

Figure 3.11: Percentage of area covered with the last 5000 time units ($m = 25$).

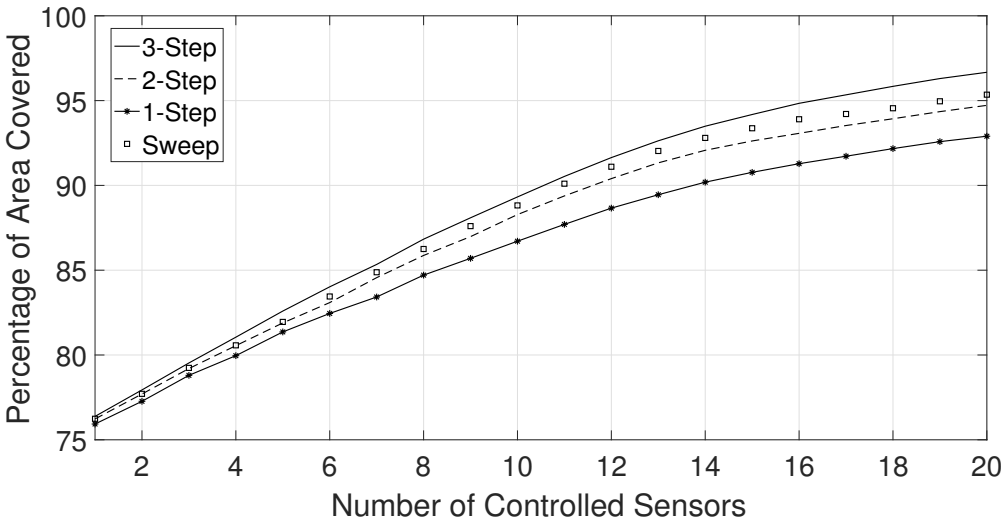

Figure 3.12: Percentage of area covered with the last 5000 time units ($m = 40$).

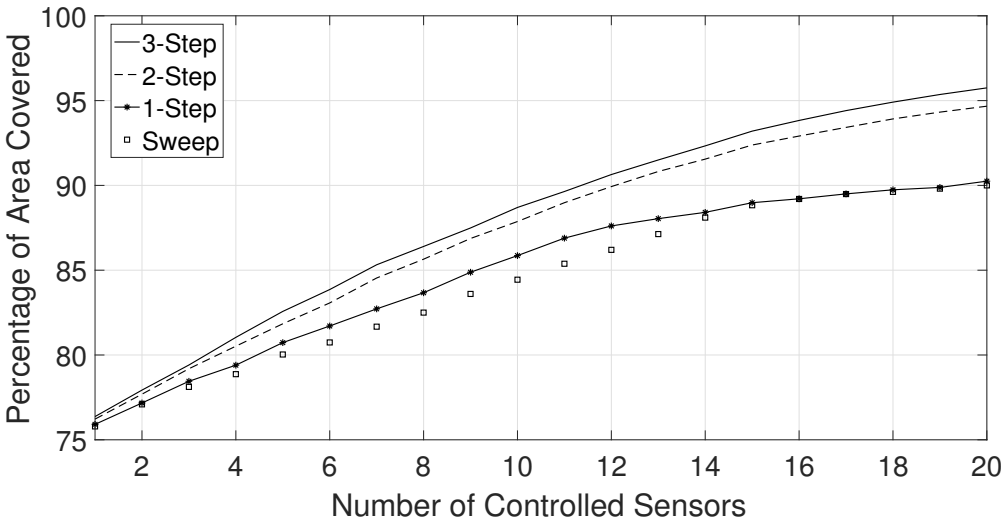

Figure 3.13: Percentage of area covered with the last 5000 time units ($m = 80$).

3.3.5 Performance of Sensor Network with Different Dimensions of Sub-regions

In this section, we compare the performance of the movement strategies under different dimensions of sub-regions. Three dimensions are shown in each figure. The three-step neighborhood movement strategy, two-step neighborhood movement strategy, one-step neighborhood movement strategy and sweep approach are all considered. Simulation results are shown in Figs. 3.14 through 3.17. The results show that $m = 40$ performs the best with all the movement strategies. The ranking of performance of $m = 80$ versus $m = 25$ depends on which movement strategy is used. In particular, the sweep strategy performs especially poorly when $m = 80$. Based on all the results presented, the three-step strategy with $m = 40$ is the best overall choice.

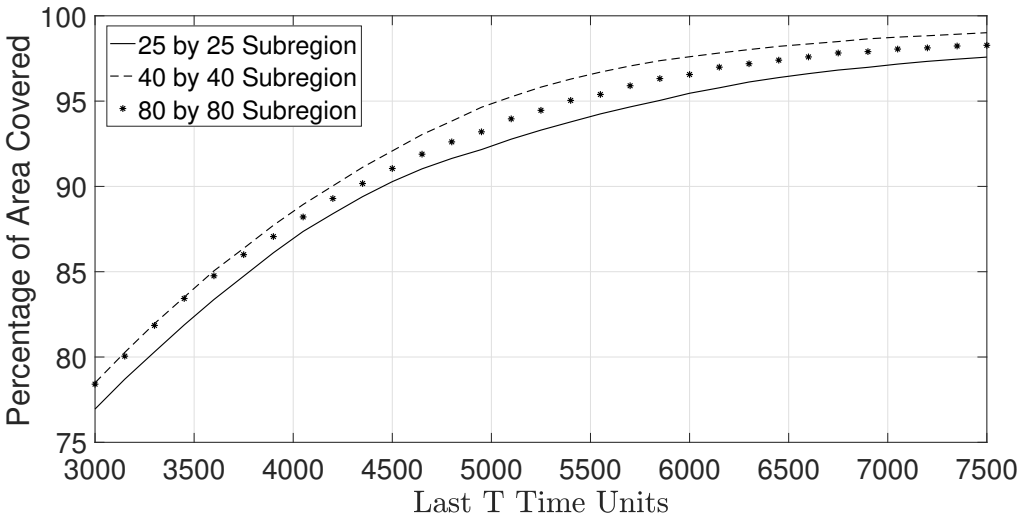

Figure 3.14: Percentage of area covered with the last T time units (three-step).

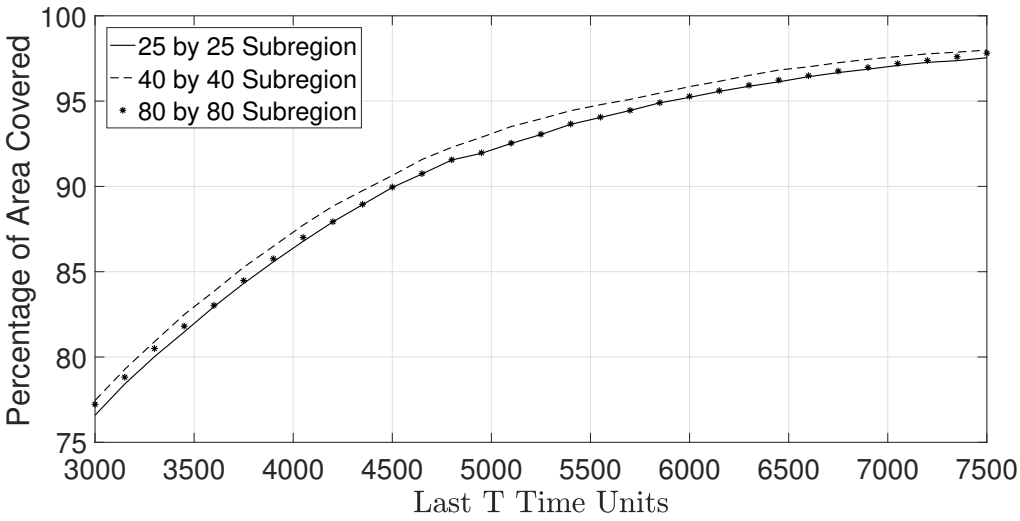

Figure 3.15: Percentage of area covered with the last T time units (two-step).

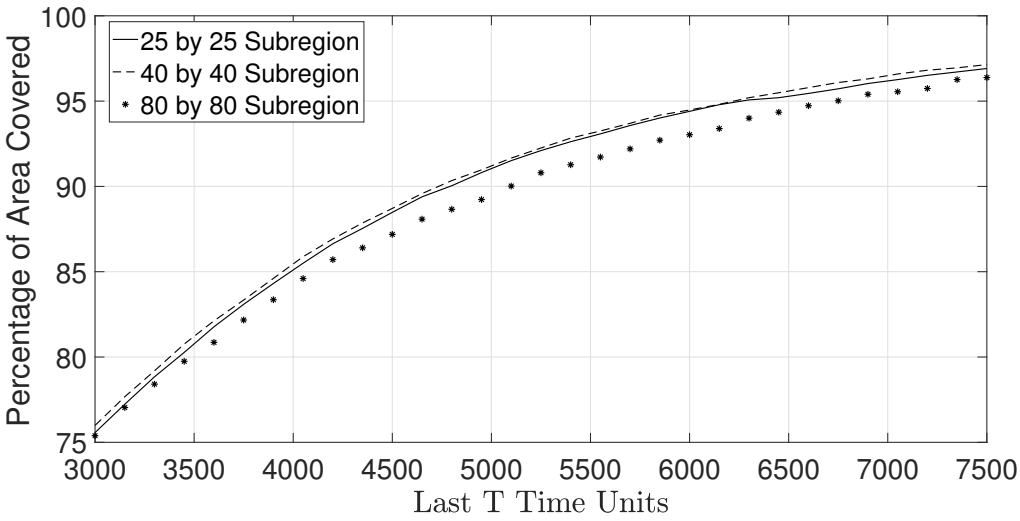

Figure 3.16: Percentage of area covered with the last T time units (one-step).

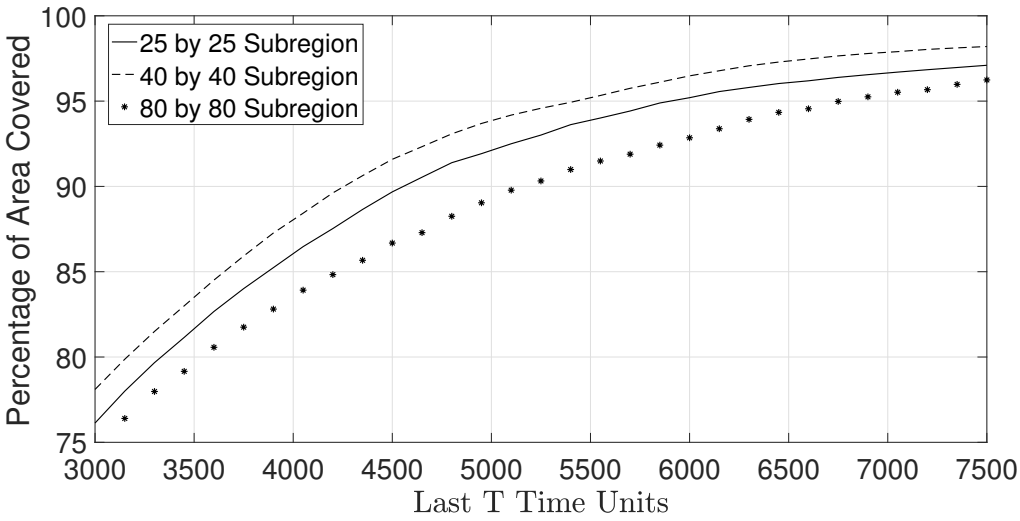

Figure 3.17: Percentage of area covered with the last T time units (sweep).

3.3.6 Performance of Sensor Network with Dynamic Number of Controlled Sensors K

In the non-dynamic approach, when a controlled sensor finishes up with a sub-region, it moves to the sub-region with the largest sum (or largest maximum value) of time since last visited. To make this approach dynamic, we instead utilize a fixed threshold τ and determine all the sub-regions in which the sum (or maximum value) of times since last visited is greater than τ. If there are zero such sub-regions, we "retire" the controlled sensor and let it operate again as an uncontrolled sensor (i.e., as a taxicab for hire to customers). If there is one such sub-region, we simply send the controlled sensor to that sub-region (which is the same as the non-dynamic algorithm). If there are W such sub-regions, where $W \geq 2$, we then "hire" $(W - 1)$ additional uncontrolled sensors to operate as controlled sensors so that all sub-regions with value greater than τ can be investigated simultaneously. We then effectively hire the taxicabs to take the path we specify without customers; that is , we hire them to go exactly where we say.

Figs. 3.18 through 3.20 present the average number of controlled sensors used as as function of the threshold τ for the three sub-region sizes $m = 25$, $m = 40$, and $m = 80$, respectively. All results assume the three-step algorithm is employed with the Worst Sum metric. The worst pixel path is used to move between sub-regions, and newly hired controlled sensors must wait until an uncontrolled sensor finishes its current path.

As expected, the average number of controlled sensors decreases as τ increases; indeed, there would be zero controlled sensors if τ equaled infinity, because the Worst Sum metric could never exceed τ in that case.

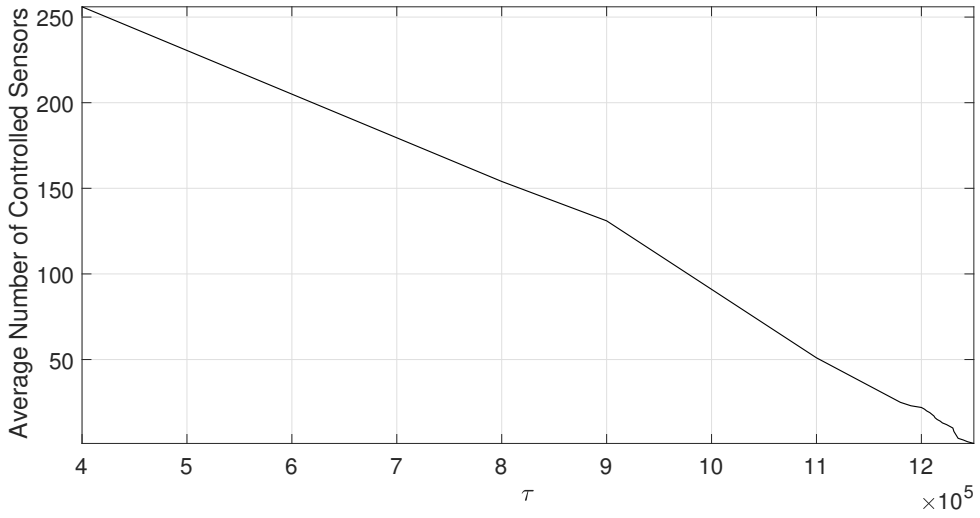

Figure 3.18: Average number of controlled sensors with threshold τ ($m = 25$).

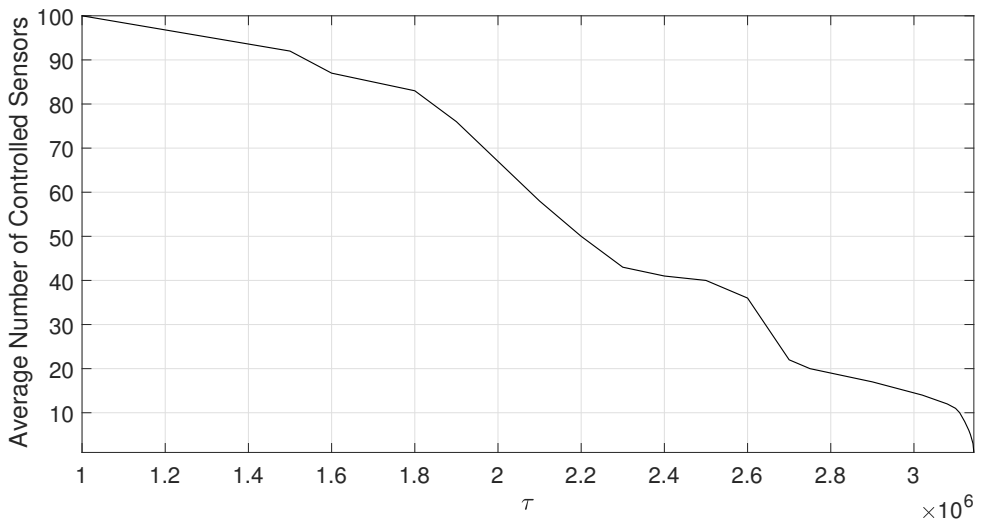

Figure 3.19: Average number of controlled sensors with threshold τ ($m = 40$).

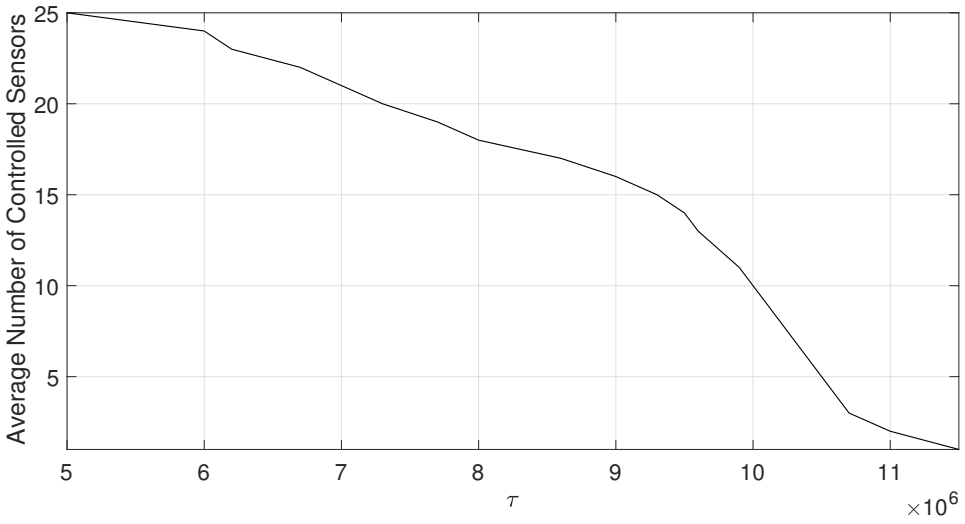

Figure 3.20: Average number of controlled sensors with threshold τ ($m = 80$).

Figs. 3.21 through 3.23 present a comparison of the dynamic and non-dynamic algorithms as a function of the average number of controlled sensors. (For the non-dynamic algorithm this "average" number is fixed for all time; only the dynamic algorithm has a time-varying number of controlled sensors.) For the dynamic algorithm, we select the average number of controlled sensors through our choice of the threshold τ, as indicated by the results of Figs. 3.18 through 3.20.

The result of Figs. 3.21 through 3.23 show that, regardless of the sub-region size, the dynamic algorithm significantly outperforms the non-dynamic algorithm. Fig. 3.24 compares the three sub-region sizes and again shows that the 40 by 40 sub-region size gives the best performance.

Note that the gains of the adaptive algorithm come at the cost of hiring additional sensors as needed. Hiring a taxicab is likely to be significantly more expensive than utilizing vehicles to operate as dedicated controlled sensors.

3.4 Conclusions

In this chapter, we have described algorithms for hybrid mobile sensor networks designed to provide consistent surveillance of a metropolitan area. The results show that the three-step movement, global assignment and worst sum metrics all combine to make hybrid sensor networks significantly outperform networks that do not use controlled sensors. Furthermore, by applying dynamic controlled sensors, the performance of the network increases significantly, although at increased operational cost.

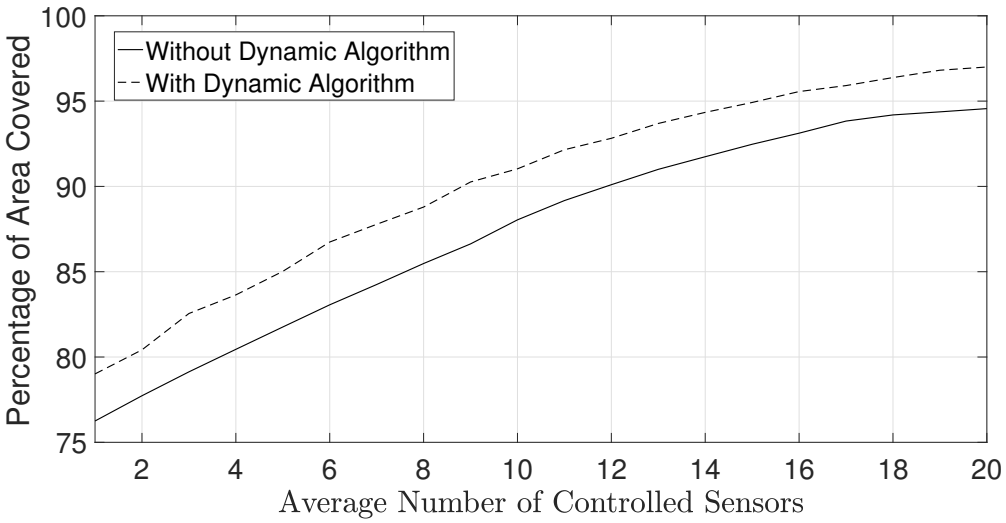

Figure 3.21: Percentage of area covered with the last 5000 time units ($m = 25$).

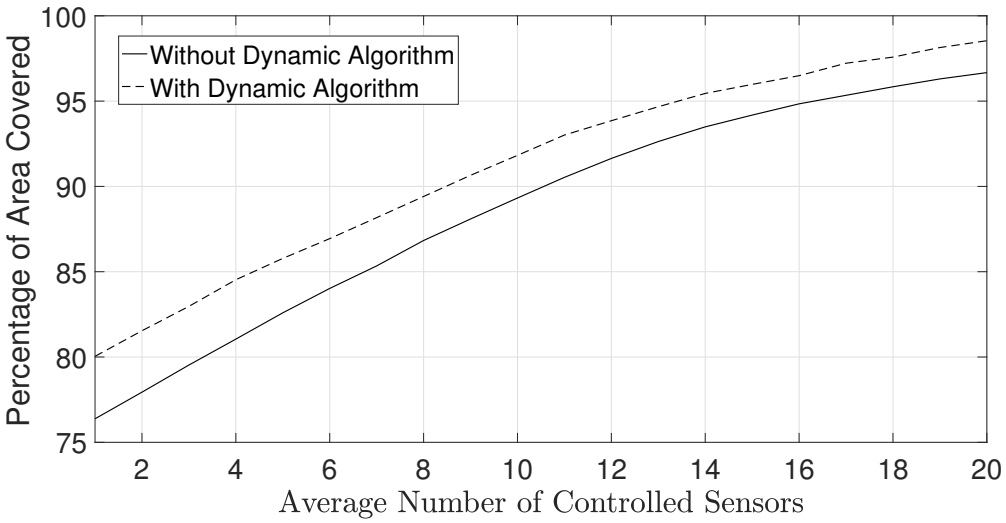

Figure 3.22: Percentage of area covered with the last 5000 time units ($m = 40$).

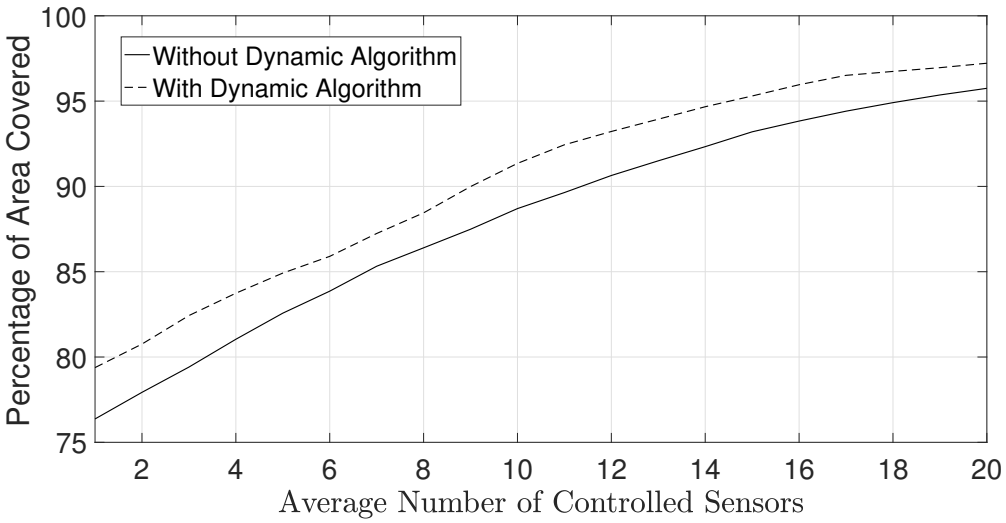

Figure 3.23: Percentage of area covered with the last 5000 time units ($m = 80$).

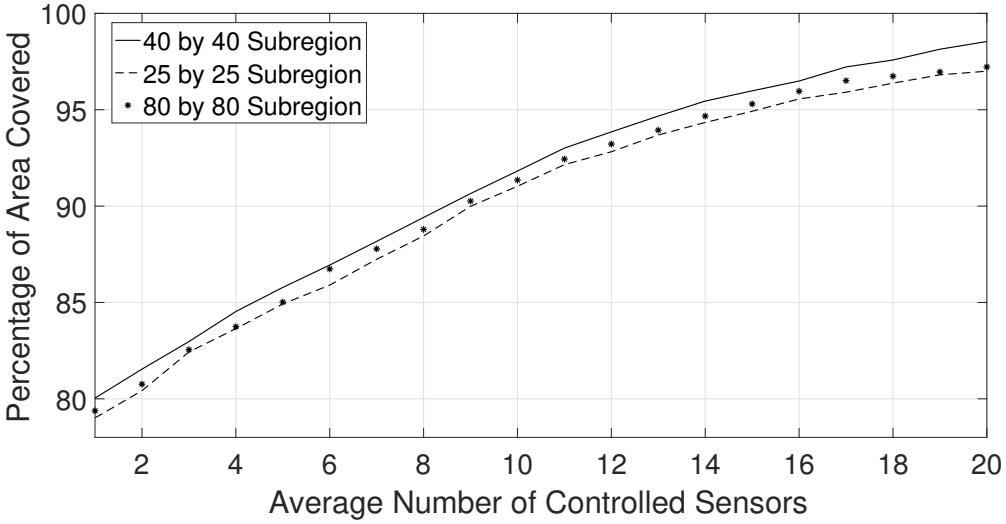

Figure 3.24: Percentage of area covered with the last 5000 time units with dynamic algorithm.

Chapter 4

Sensor Search Strategies Exploiting Probabilistic Modeling

In this chapter, we incorporate the probability-based detection models of Chapter 2 into the simulation framework of Chapter 3. These more realistic models will also by necessity incorporate models for the speed of vehicles performing surveillance. A sensor moving at low speeds can have a lower probability of miss than one moving at high speeds if there is a radiation source nearby. We therefore believe that we can significantly improve the performance of our algorithm by exploiting velocity information. One approach is to model a "smallest" source we wish to detect and, based on velocity and path information, calculate the probability of missing a source of this size in each block. This information can be incorporated into a secondary array akin to the Real-Time Coverage Information Array to make better global assignments and better sub-region movement strategies as well.

4.1 Detection Theory with Probability of Miss of Static Radiation Source

To incorporate the detection performance models of Chapter 2 to the surveillance of metropolitan areas, Equation (2.33) is applied to calculate the probability of miss when a detector moves along a straight path and there is a fixed radiation source nearby. As a controlled sensor moves in the metropolitan area, the probability of miss can be calculated with information on the source strength, speed of vehicle, distance between the source and the vehicle and the detection path.

In our modeling of the Real-Time Coverage Information Array, sensors are modeled as moving from the center of one block horizontally or vertically to the center of an adjoining block. As a worst case, we model possible source locations at the corner of a block. This is indeed a worst case in the sense that if a bock has length L, the closest a sensor can ever get is $L/2$, assuming the source is at ground level. (We assume the source is at ground level in all that follows. To model a source at height h, one should again use Equation (2.33) but with different parameters; in this case the closest a sensor traveling on the ground can get to the source is $\sqrt{h^2 + L^2/4}$). As a worst case in this situation one could take h to be the height of the tallest building in a given metropolitan area. However, we do not expect the general performance observations we obtain to change significantly by incorporating a height h).

Consider the situation shown in Fig. 4.1; only a portion of the overall grid is shown. A sensor is located in the middle of the center square, indicated by the coordinate (17,42). Each corner location (sixteen are shown) is a hypothesized location of a nuclear source. The quantity $P(i,j)[n]$ denotes the probability of miss at time slot n if the source is at corner coordinate (i,j). (Our convention is that for a given block, the sensor-based coordinates of the block match the source location of the upper left corner of the block). Note that if no sensor ever passes close to location (i,j), the quantity $P(i,j)[n]$ will be very large, close to one. If instead many sensors frequently pass close to location (i,j), the quantity $P(i,j)[n]$

will be very small, close to zero.

Now consider the situation shown in Fig. 4.2, in which the sensor in Fig. 4.1 moves horizontally to the right over one time slot. This action will require that each probability be updated by multiplying it by a term of the form of Equation (2.33). For example, examination of the geometries of Fig. 4.2 and Fig. 2.5 shows that

$$P(17,42)[155] = P(17,42)[154]P_M^L(L/2; L/2, 3L/2)$$

and

$$P(16,41)[155] = P(16,41)[154]P_M^L(3L/2; 3L/2, 5L/2)$$

where $P_M^L(\ell; r_1, r_2)$ is given by Equation (2.33). Note that $P_M^L(\ell; r_1, r_2)$, in addition to geometric parameters ℓ, r_1, and r_2, also depends on C, the strength of the source, v, the speed of the sensor, and ρ, the air attenuation coefficient. (In practice, buildings and other solid objects may cause additional attenuation, but because we are only trying to detect a source to the nearest city block, we do not expect this additional attenuation to change the general nature of our results.)

As multiple controlled and uncontrolled sensors move around the grid, the matrix of probability $P(i,j)[n]$ will change continually. As a practical matter, only the source locations close to a given sensor will change much as the sensor moves, because for greater distance the probability of miss is close to one. Note that this Real-Time Detection Array enables us to more accurately model a mobile sensor than the simpler zero-one model of Chapter 3. However, the Real-Time Coverage Information Array is still useful in conjunction with the Detection Array, because it is still important to know how long it has been since a block has been visited. Because a nuclear source may suddenly appear (for example, removed from a container in order to arm a "dirty bomb"), probability data may not be meaningful if previous visits, although numerous, happened an extremely long time ago.

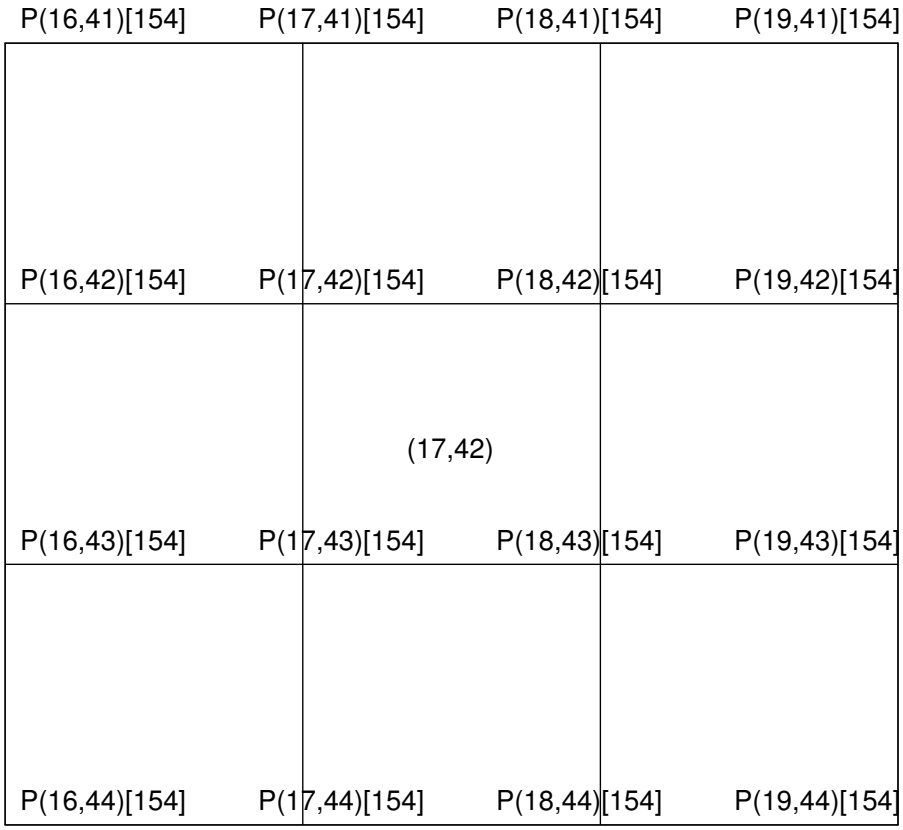

Figure 4.1: Sensor location in middle of center block.

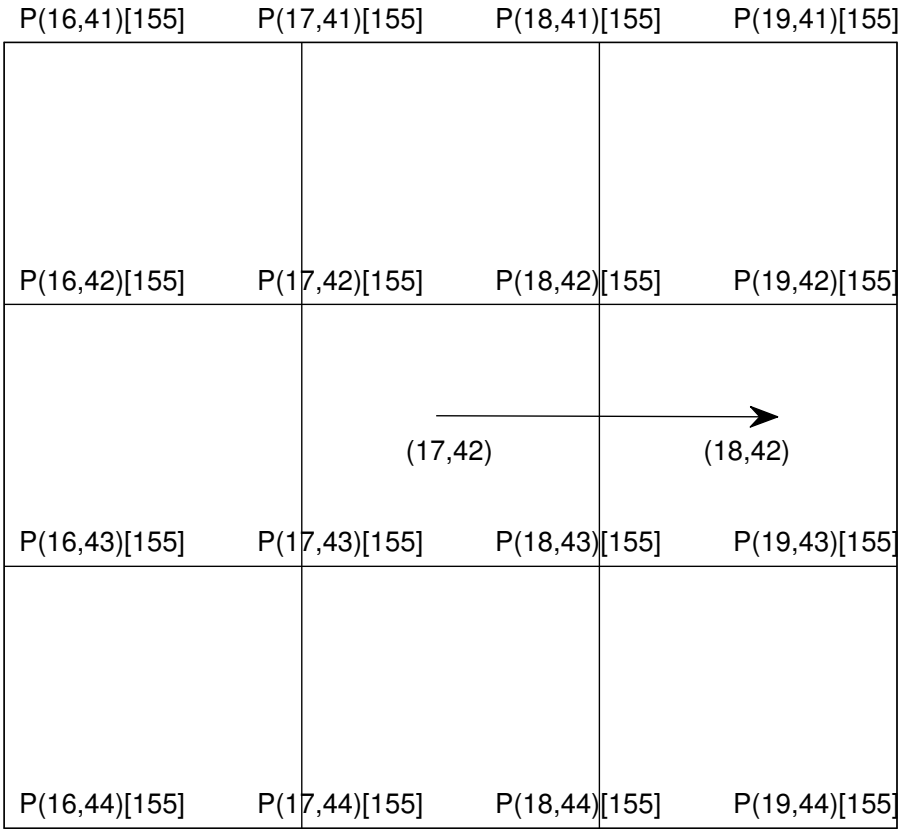

Figure 4.2: Sensor move from center block to immediate right block.

4.2 Time and Probability-based Detection Algorithm

The probability information stored in the Real-Time Detection Array can be computed by a central controller if the GPS data of each mobile sensor is related to this controller. (Note that average velocity information over a block can be determined from GPS time and position information.) The only quantity that is not known is the strength of the source. In order to guarantee that miss probabilities are not worst than computed, one can choose a worst-case source strength. (Note that worst case, in this context, means a small, weak source, because a stronger source is easier to detect.)

How should this information be utilized? In the algorithms described in Chapter 3, there are two critical questions: where to go within a sub-region (e.g., utilizing the three-step neighborhood movement strategy) and, when finishing with a sub-region, what sub-region to go to next. We can utilize the Real-Time Detection Array to assist with the first of these tasks. Within the three-step neighborhood movement strategy, instead of basing our decision of where to go next on the sums of times since last being visited, we base this decision on sums of probabilities of neighborhood sources. For a given three-step path we utilize all of the probability values on the corners of the path. As can be seen in Fig. 4.3, there are always ten such corners located on a three-step path. The decision of where to move next is based on the direction that has the largest such sum of ten values.

As to the question of what sub-region a sensor should visit after completing a sub-region, we choose to base this decision on time information alone in the manner of Chapter 3. For reasons already explained, it is important that time information not be neglected at the expense of probability information. Basing sub-region assignment on time information ensures that all portions of the metropolitan area are visited with regularity.

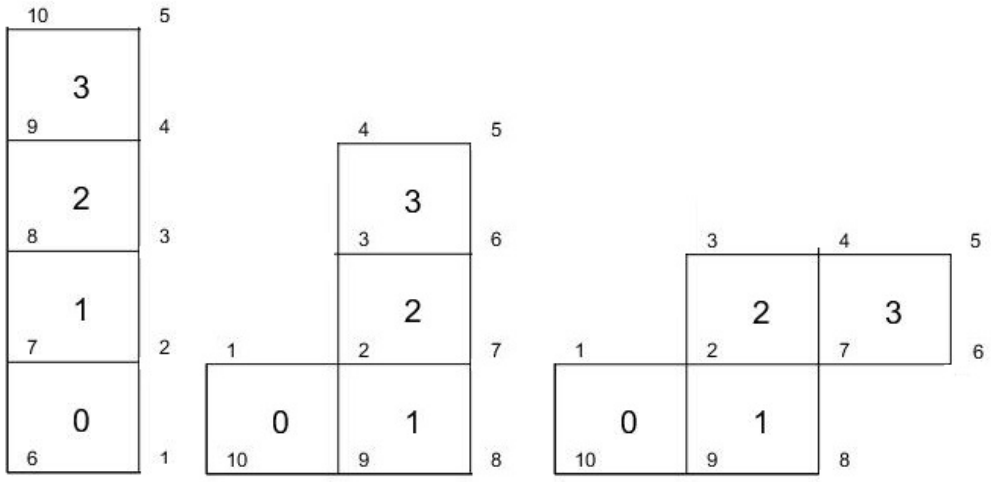

Figure 4.3: Three-step paths and corner locations.

4.3 Simulation of Detection with Probabilistic Models

Our simulation employs the models and parameters of Chapter 3. however, we base performance on the percentage of the area for which the probability of miss is less than a threshold α. As the area is divided into N^2 grid blocks, the size of the Real-Time Detection Array is $(N+1)^2$. As with Chapter 3, we set $N = 400$. One additional generalization of the model is that we assume each vehicle (both controlled and uncontrolled sensors) randomly moves from block to block at speeds of 40 mph, 30 mph and 20mph (64.4 kmph, 48.3 kmph, and 32.2 kmph), each with equal probability, independent from block to block. In order to implement variable velocity in a time-slotted system, we subdivide our basic time unit into 12 time chips, so that moving to the next block requires 6 time chips at 20 mph, 4 time chips at 30 mph, and 3 time chips at 40 mph. Because only nearby source locations are meaningfully affected by a given sensor, we only update the 16 locations in the 3 by 3 block around the sensor at any given time. For all the results presented, the simulation run length is 5,000 time slots (60,000 chips).

Figs. 4.4 through 4.6 compare the performance of both the time-based three-step movement algorithm of Chapter 3 with the time-and-probability-based algorithm of this chapter. Performance is measured by the percentage of coverage with the probability of miss less than α, where values of $\alpha = 0, 1, 0.01$, and 0.001 are considered. Fig. 4.4 assumes a source strength of $C = 1000\ m/s$. Fig. 4.5 uses $C = 2500\ m/s$, and Fig. 4.6 uses $C = 5000\ m/s$. In each case, the use of probability-based information improves the performance. The gains are most significant with a stronger source.

In Figs. 4.7 through 4.9, the dynamic controlled sensor algorithm is added. Recall that this algorithm determines whether to retire a current sensor, keep it, or hire additional controlled sensors based on how many sub-regions have worst sum value greater than a threshold. Here the horizontal axis is the average number of controlled sensors because the number of such sensors varies over time. The results show gains similar to those in the non-dynamic case.

The dynamic and non-dynamic approaches are compared using the time-based three-step movement strategy of Chapter 3 in Figs. 4.10 through 4.12, and they are compared using the time-and-probability based methods of this chapter in Figs. 4.13 through 4.15. The results show that the adaptive method consistently outperforms the non-adaptive method. The gains are especially significant when the source is strong. For example, Fig. 4.15 shows that, with six controlled sensors, the dynamic method with $\alpha = 0.01$ gives identical performance to that of the non-dynamic method of $\alpha = 0.1$; that is, use of the dynamic method enables a factor of ten reduction in the worst case miss probability.

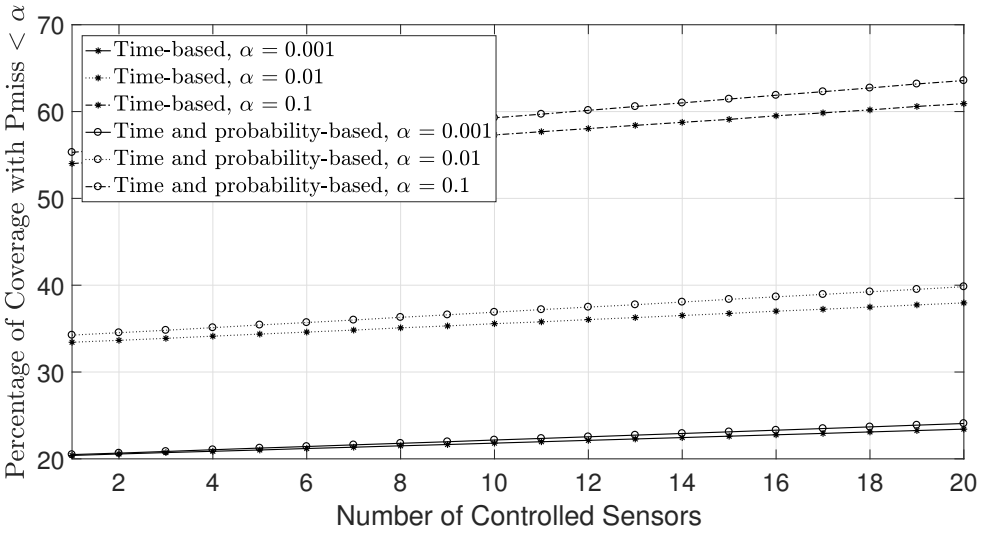

Figure 4.4: Comparison of time-based and time-and-probability-based three-step movement, $C = 1000$ m/s.

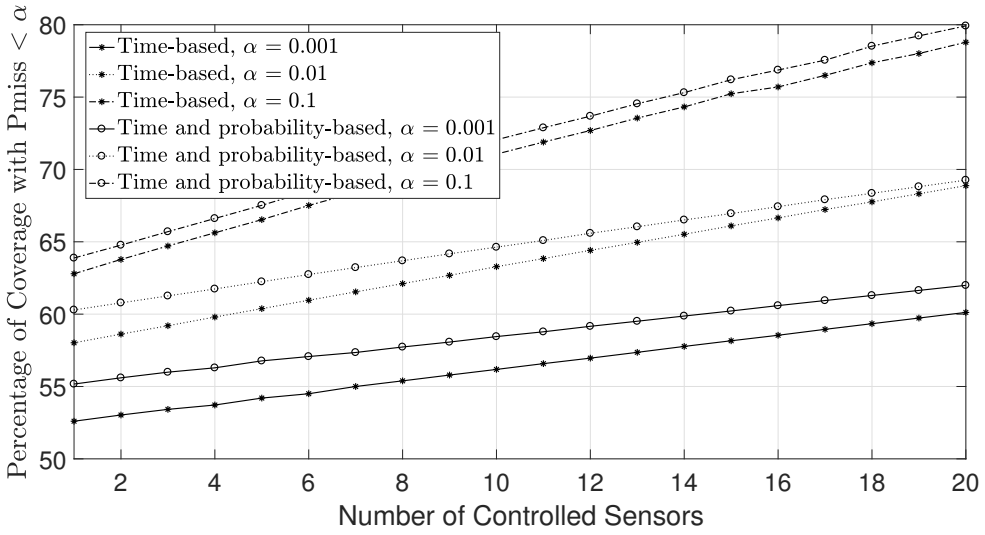

Figure 4.5: Comparison of time-based and time-and-probability-based three-step movement, $C = 2500$ m/s.

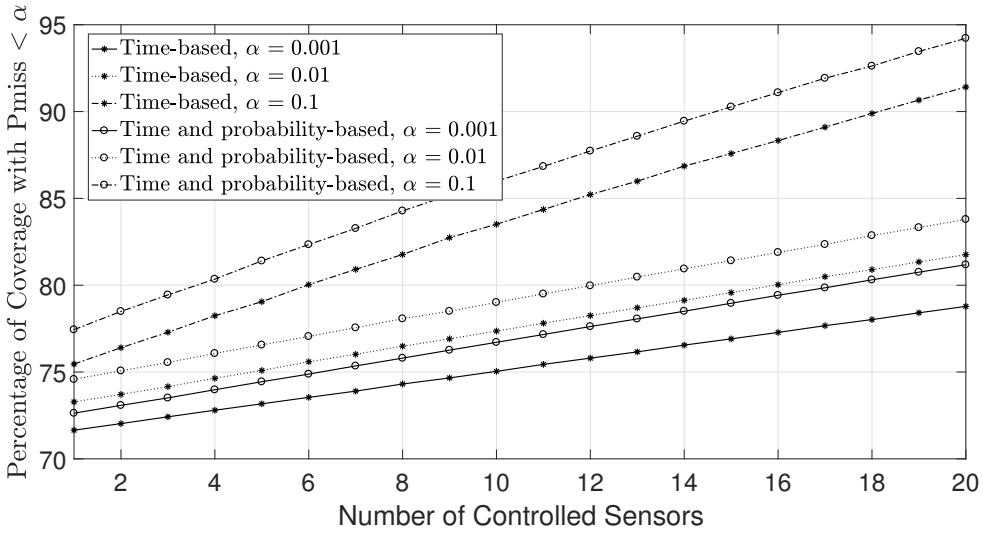

Figure 4.6: Comparison of time-based and time-and-probability-based three-step movement, $C = 5000$ m/s.

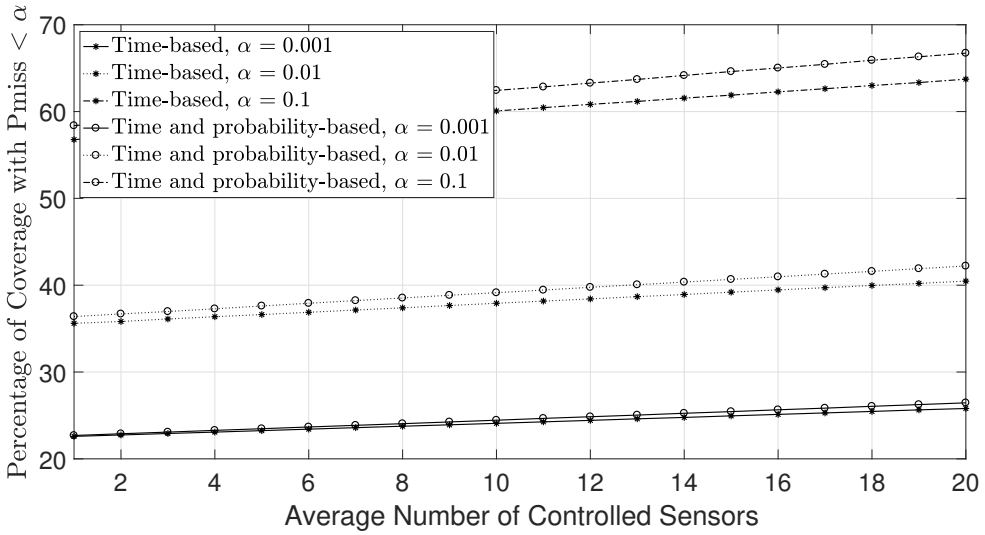

Figure 4.7: Comparison of time-based and time-and-probability-based three-step movement, dynamic sensor assignment, $C = 1000$ m/s.

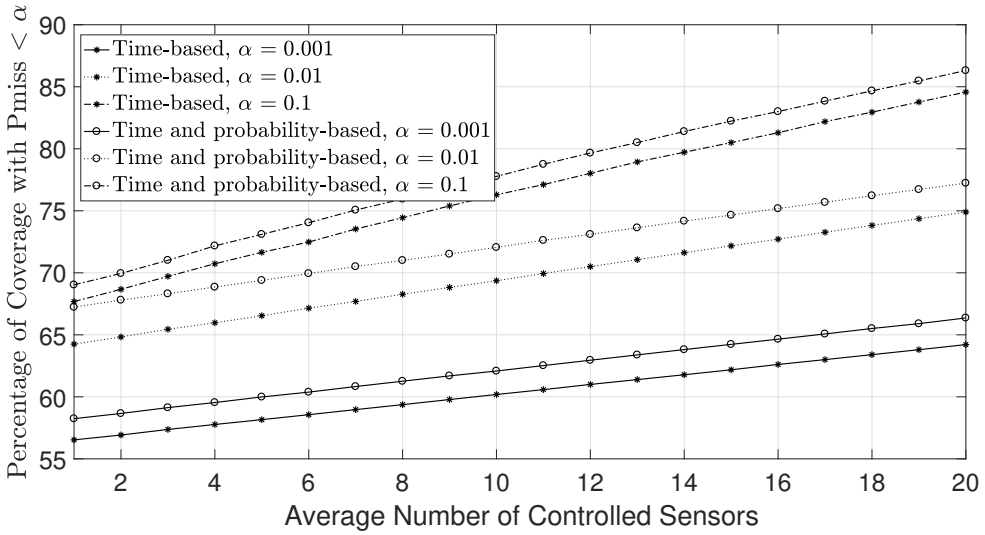

Figure 4.8: Comparison of time-based and time-and-probability-based three-step movement, dynamic sensor assignment, $C = 2500$ m/s.

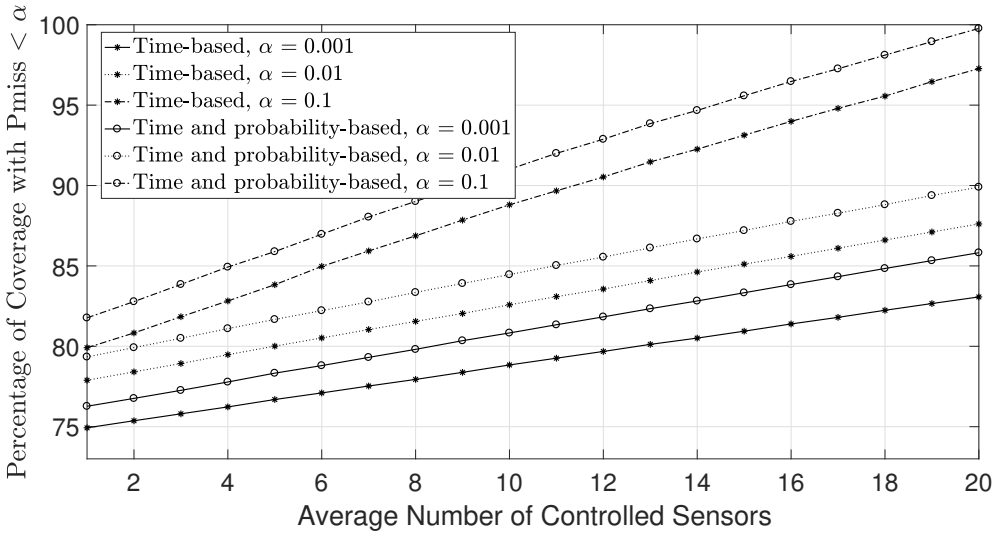

Figure 4.9: Comparison of time-based and time-and-probability-based three-step movement, dynamic sensor assignment, $C = 5000$ m/s.

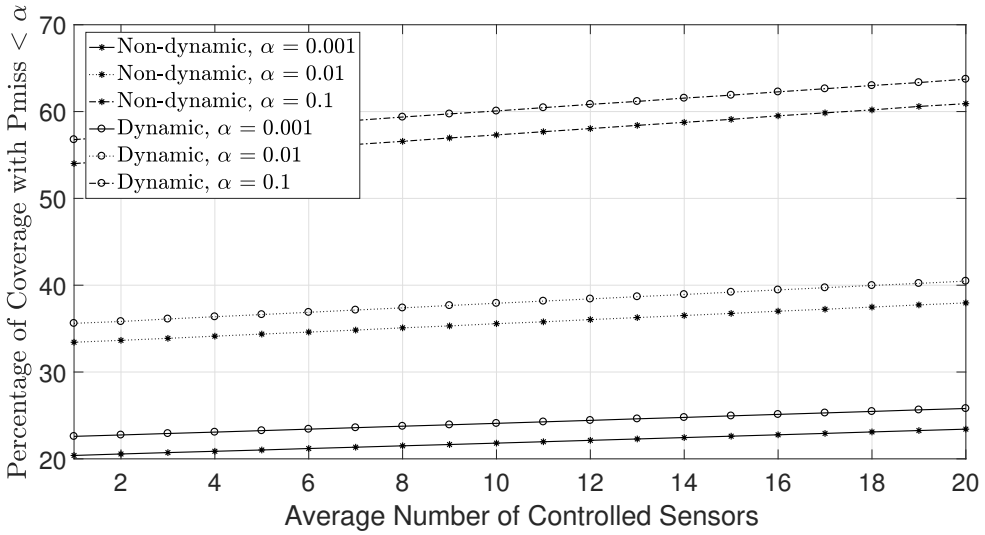

Figure 4.10: Comparison of dynamic and non-dynamic three-step movement, time-based three-step movement, $C = 1000$ m/s.

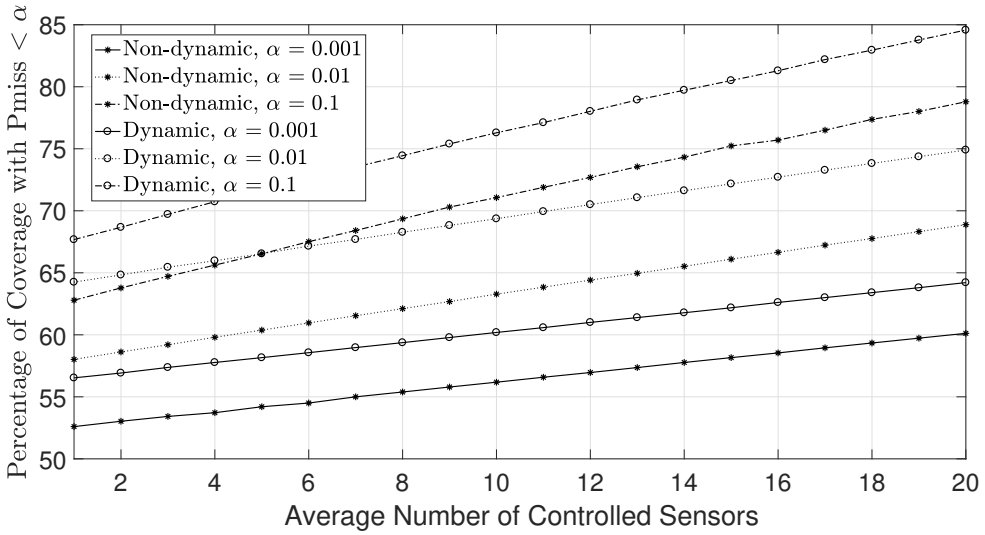

Figure 4.11: Comparison of dynamic and non-dynamic three-step movement, time-based three-step movement, $C = 2500$ m/s.

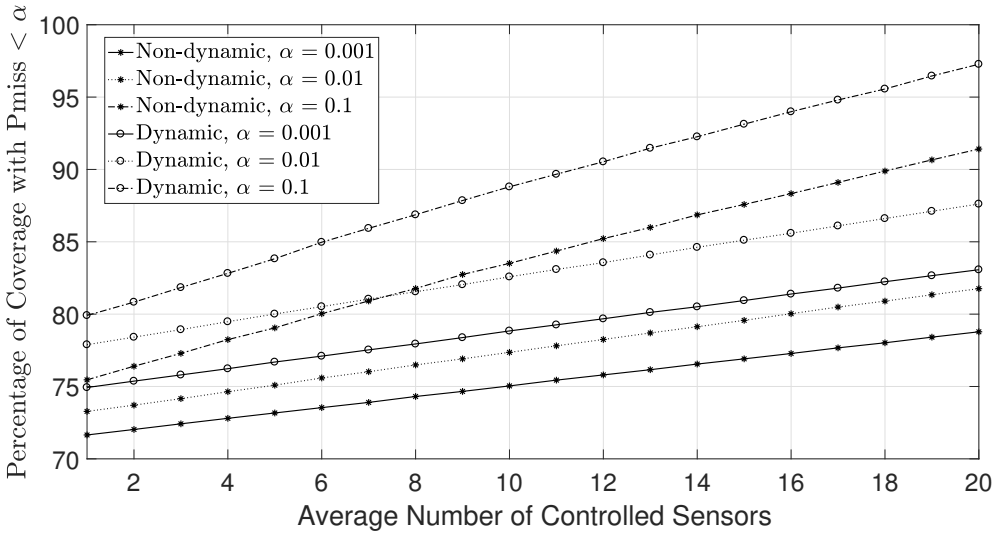

Figure 4.12: Comparison of dynamic and non-dynamic three-step movement, time-based three-step movement, $C = 5000$ m/s.

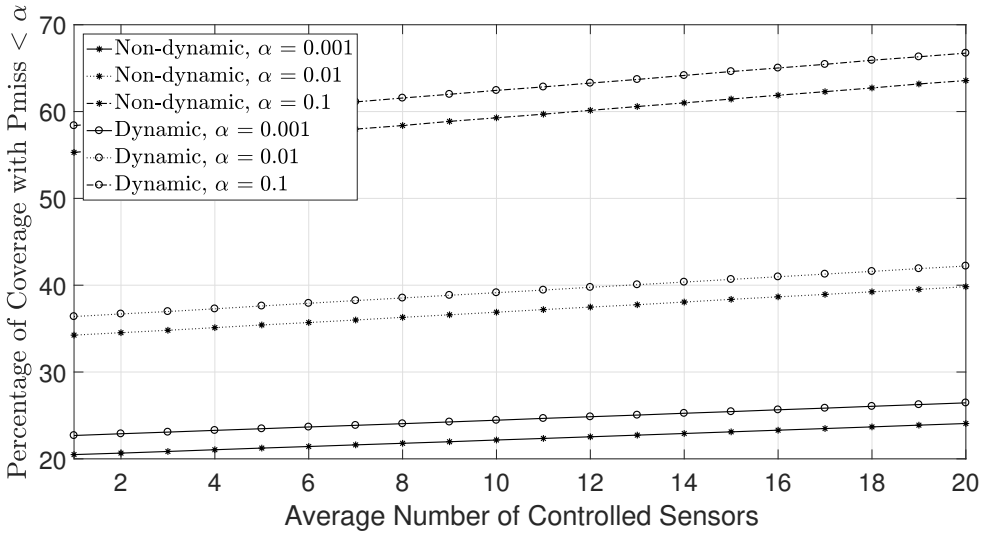

Figure 4.13: Comparison of dynamic and non-dynamic three-step movement, time-and-probability-based three-step movement, $C = 1000$ m/s.

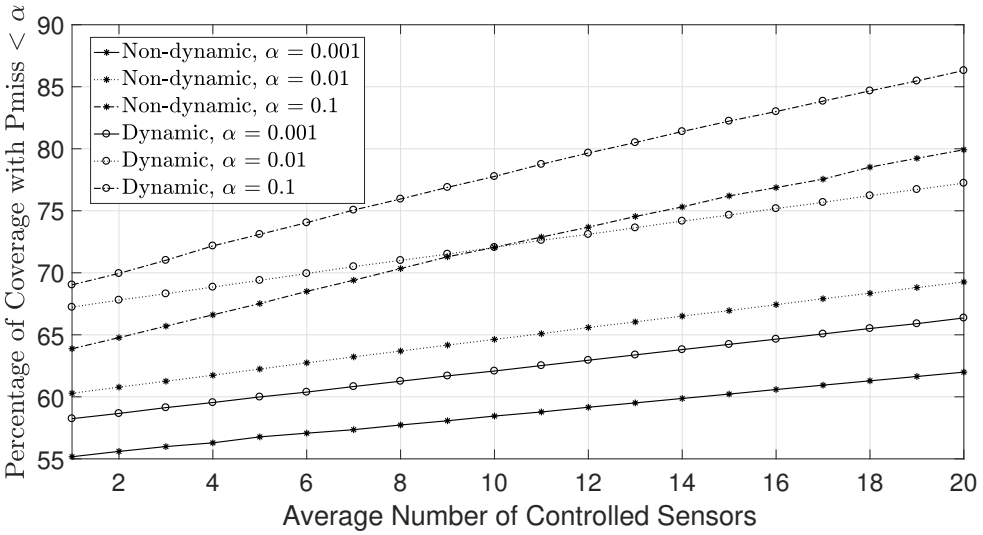

Figure 4.14: Comparison of dynamic and non-dynamic three-step movement, time-and-probability-based three-step movement, $C = 2500$ m/s.

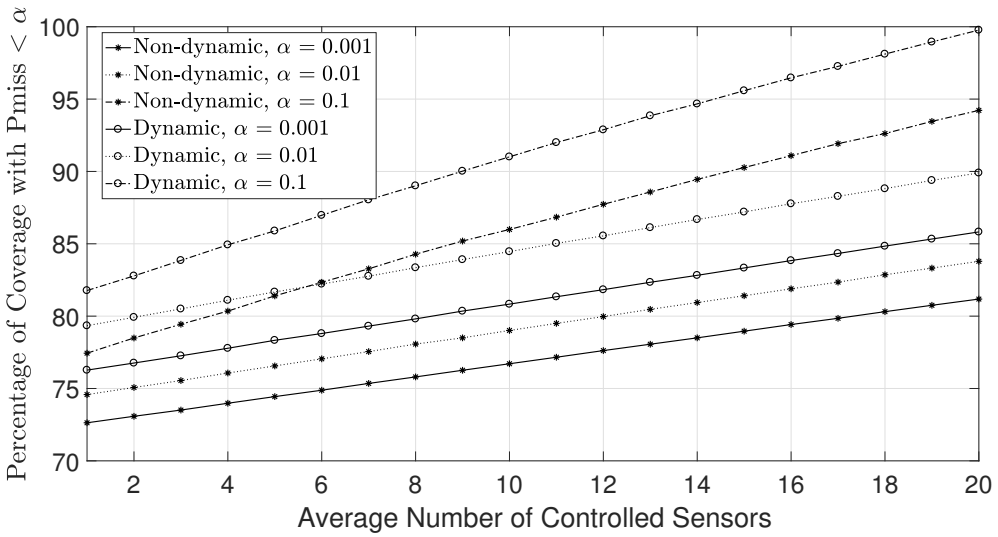

Figure 4.15: Comparison of dynamic and non-dynamic three-step movement, time-and-probability-based three-step movement, $C = 5000$ m/s.

4.4 Conclusions

In this chapter a probabilistic method for analyzing the performance of sensor search strategies has been presented and applied to the algorithms of Chapter 3. The model exploits the probability of miss for mobile sensors developed in Chapter 2. In addition, an approach to sensor movement within a sub-region has been presented that exploits this information which can be readily calculated by a central controller using GPS information from all sensors.

Chapter 5

Conclusions and Future Work

In this work, we focus on the detection analysis and search strategies for nuclear radiation sources. Expanding on previous research, we propose the use of a hybrid mobile sensor network that uses time information and probability information to guide the deployment of the sensor network.

In Chapter 2, we introduce novel analytical techniques that enable the calculation of the probability of miss for a mobile sensor detecting a stationary nuclear source. Various patterns of the sensor's movement are studied, including linear, circular, and rectangular movement. Both two- and three-dimensional geometries have been analyzed. To better understand the detection model, we also perform Bayesian analysis. The analytical techniques provide a way to simply estimate the effects of movement pattern, speed, source strength, and the absorption profile, and as a result, the analysis is widely applicable to many scenarios involving nuclear detection with mobility.

In Chapter 3, we introduce sub-regions and assignment strategies to perform surveillance with hybrid mobile sensor network. Global assignment and local assignment strategies are compared and results show that global assignment outperforms local assignment. Also, it is shown that movement strategies that exploit the fact that uncontrolled sensors haphazardly and sparsely cover a region (specifically, the three-step movement strategy) can

outperform strategies that ignore this fact (the sweep strategy). In addition, it is shown that well-designed dynamic algorithms that "hire" additional controlled sensors as needed significantly outperform algorithms that utilize a static number of controlled sensors.

In Chapter 4, the detection model of Chapter 2 is applied to the search strategies of Chapter 3 to show that the conclusions of Chapter 3 still hold when this more accurate analysis is employed. Because the probability of miss calculations only require knowledge of parameters known to the central controller, we propose a new movement strategy that exploits probabilistic information. It is shown that this movement strategy results in sensor network performance that significantly outperforms the time-based strategies of Chapter 3.

Multiple opportunities exist to extend this work. One area is to explore how to incorporate background radiation into the analysis of Chapter 2. Another is to explore how to incorporate probability information into where a sensor should go after completing a sub-region search. Also of value is to explore how to incorporate probability information into the dynamic algorithm for deciding when to hire and retire additional random sensors to serve temporarily as controlled sensors. Finally, this work is preliminary in the sense that it presumes a square grid with unlimited access. It is important to extend the work for arbitrary metropolitan area geometries and also incorporate other practical conditions such as non-uniform traffic, street widths, speed limits, traffic lights, etc.

Bibliography

[1] Budhaditya Deb. *Iterative Estimation of Location and Trajectory of Radioactive Sources With a Networked System of Detectors*. IEEE Transactions on Nuclear Science, Vol. 60, No. 2, Apr. 2013.

[2] S. V. Nageswara Rao, J.C.Chin, D.K. Yau,S. Srivathsan,S.S. Iyengar, Y. Yang, J. C. Hou, X. Xu, and S. Sahni. *Identification of low-level point radiation sources using a sensor network* in Proc. Int. Conf. Inf.Process. in Sensor Networks, 2008.

[3] S. V. NageswaraRao, J. C. Chin, D. K. Y. Yau, Y. Yang, J. C. Hou, X. Xu, and S. Sahni. *Localization under random measurements with application to radiation sources* in Proc. Int. Conf. Inf. Fusion, 2008.

[4] H. Zhang and J. Hou. *Is deterministic deployment worse than random deployment for wireless sensor networks?*. in Proc. IEEE INFOCOM, Apr. 2006.

[5] X. Bai, S. Kumar, D. Xuan, Z. Yun, and T. H. Lai. *Deploying wireless sensors to achieve both coverage and connectivity* in Proc. 7th ACM Int. Symp. MobiHoc, May 2006, pp. 131142.

[6] M. Ma and Y. Yang. *Adaptive triangular deployment algorithm for unattended mobile sensor networks* IEEE Trans. Comput., Vol. 56, No. 7, pp. 946958, Jul. 2007.

[7] C.-Y. Chang, C.-T. Chang, Y.-C. Chen, and H.-R. Chang. *Obstacleresistant deployment algorithms for wireless sensor networks* IEEE Trans. Veh. Technol., Vol. 58, No. 6, pp. 29252941, Jul. 2009.

[8] Seapahn Meguerdichian1, Farinaz Koushanfar, Miodrag Potkonjak1, Mani B. Srivastava. *Coverage Problems in Wireless Ad-hoc Sensor Networks*

[9] S. Shakkottai, R. Srikant, and N. Shroff. *Unreliable sensor grids: Coverage, connectivity and diameter* In Proc. IEEE Infocom, 2003.

[10] B. Liu and D. Towsley. *A study on the coverage of large-scale sensor networks* In The 1st IEEE International Conference on Mobile Ad-hoc and Sensor Systems, 2004.

[11] G. Wang, G. Cao, and T. F. La Porta. *Movement-assisted sensor deployment* IEEE Trans.Mobile Comput., Vol. 5, No. 6, pp. 640652, Jun. 2006.

[12] B. Wang, H. B. Lim, and D. Ma. *A survey of movement strategies for improving network coverage in wireless sensor networks* Comput. Commun., Vol. 32, No. 13/14, pp. 14271436, Aug. 2009.

[13] Y.-C.Wang, C.-C. Hu, and Y.-C. Tseng. *Efficient placement and dispatch of sensors in a wireless sensor network* IEEE Trans. Mobile Comput., Vol. 7, No. 2, pp. 262274, Feb. 2008.

[14] J. Wu and S. Yang. *SMART: A scan-based movement-assisted sensor deployment method in wireless sensor networks*

[15] T. Clouqueur, V. Phipatanasuphorn, P. Ramanathan, and K. K. Saluja. *Sensor deployment stategy for target detection* In First ACM International Workshop on Wireless Sensor Networks and Applications, 2002.

[16] Zhong Shen, Yilin Chang, Hai Jiang, Yanling Wang, Zhongjiang Yan. *A Generic Framework for Optimal Mobile Sensor Redeployment* IEEE Transactions on Vehicular Technology, Vol. 59, No. 8, Oct. 2010

[17] S. Chellappan,W. Gu, X. Bai, D. Xuan, B.Ma, and K. Zhang. *Deploying wireless sensor networks under limited mobility constraints* IEEE Trans. Mobile Comput., Vol. 6, No. 10, pp. 11421157, Oct. 2007.

[18] I. I. Hussein and D. Stipanovic. *Effective Coverage Control using Dynamic Sensor Networks* 2006 IEEE Conference on Decision and Control, pp. 2747 2752, December 2006.

[19] Islam I. Hussein and Dusan M. Stipanovic. *Effective Coverage Control for Mobile Sensor Networks with Guaranteed Collision Avoidance* IEEE Transactions on Control Systems Technology, Special Issue on Multi-Vehicle Systems Cooperative Control with Applications, Vol. 15, No. 4, pp. 642 657, 2007.

[20] S. Meguerdichian, F. Koushanfar, M. Potkonjak, and M. B. Srivastava. *Coverage problems in wireless ad-hoc sensor networks* In Proc. IEEE Infocom, pages 13801387, 2001.

[21] J. C. Latombe, A. Lazanas, and S. Shekhar. *Robot motion planning with uncertainty in control and sensing* Artificial Intelligence, 52 (1991), pp. 147.

[22] E. U. Acar and H. Choset. *Sensor-based coverage of unknown environments: Incremental construction of morse decompositions* International Journal of Robotics Research, Vol. 21, No. 4, pp. 345 366, 2002.

[23] Jerry Cheng, Minge Xie and Rong Chen, Fred Roberts,DIMACS. *A Mobile Sensor Network for the Surveillance of Nuclear Materials in Metropolitan Areas* DIMACS Technical Report 2009-19 August 2009.

[24] Jerry Cheng, Minge Xie and Fred Roberts. *Design and Deployment of a Mobile sensor network for the Surveillance of Nuclear Materials in Metropolitan Areas*

[25] A. Howard, M. J. Mataric, and G. S. Sukhatme. *Mobile sensor network deployment using potential fields: A distributed scalable solution to the area coverage problem* in Proc. 6th Int. Symp. DARS, Jun. 2002, pp. 299308.

[26] Y. Zou and K. Chakrabarty. *Sensor deployment and target localization based on virtual forces* in Proc. IEEE INFOCOM, Mar./Apr. 2003, pp. 12931303.

[27] S. Yang, J. Wu, and F. Dai. *Localized movement-assisted sensor deployment in wireless sensor networks* in Proc. IEEE Int. Conf. MASS, Oct. 2006, pp. 753758.

[28] Dhillon, S.S., Chakrabarty, K., Iyengar, S.S. *Sensor Placement for Grid Coverage under Imprecise Detection Information Fusion* 2002. Proceedings of the Fifth International Conference on (Volume: 2).

[29] A. Okabe and A. Suzuki. *Locational optimization problems solved through Voronoi diagrams* European Journal of Operational Research, Vol. 98, No. 3, pp. 445 456, 1997.

[30] Ercan U. Acar. *Path planning for robotic demining: Robust sensor-based coverage of unstructured environments and probabilistic methods* Internat. J. Robotic Res., 22 (2003), pp. 78.

[31] Y. Zou and K. Chakrabarty. *Sensor deployment and target localization based on virtual forces* In Proc. IEEE Infocom, 2003.

[32] Gabriel M. Hoffmann, Claire J. Tomlin. *Mobile Sensor Network Control Using Mutual Information Methods and Particle Filters* IEEE Transaction on Automatic Control, Vol. 55, No. 1, Jan.2010.